MASSACHUSETTS INSTITUTE OF TECHNOLOGY

LINCOLN LABORATORY

MILLSTONE HILL THOMSON SCATTER RESULTS FOR 1965

J. V. EVANS

Group 21

TECHNICAL REPORT 474

8 DECEMBER 1969

LEXINGTON MASSACHUSETTS

The work reported in this document was performed at Lincoln Laboratory, a center for research operated by Massachusetts Institute of Technology, with the support of the Department of the Air Force under Contract AF 19(628)-5167.

ABSTRACT

This report presents F-region electron densities, and electron and ion temperatures observed during the year 1965 at the Millstone Hill Radar Observatory (42.6°N. 71.5°W) by the UHF Thomson (incoherent) scatter radar. The measurements were made over 48-hour periods that were usually scheduled to include the International Geophysical World days near the center of each month. Geomagnetic storm sudden commencements occurred during two of the observing periods, but do not appear to have given rise to marked variation of the densities or temperatures. On the other hand, measurements made during the progress of a major storm (15-19 June 1965) exhibit large changes compared with the behavior observed in the following month. The remaining months were magnetically quiet, and the density and temperature behavior were similar to those observed in 1964. Millstone is a midlatitude station exhibiting a characteristic "winter" and "summer" daytime density variation. The transition between these two types occurs rapidly around equinox, without any corresponding seasonal change in the F-region thermal structure. Current ideas concerning the mechanisms responsible for this and other features of diurnal and seasonal variations are discussed.

Accepted for the Air Force
Franklin C. Hudson
Chief, Lincoln Laboratory Office

CONTENTS

MILLSTONE HILL THOMSON SCATTER RESULTS FOR 1965

I. INTRODUCTION

This report presents the results of synoptic studies of the F-region for the year 1965 using the Thomson (incoherent) scatter radar at Millstone Hill, Westford, Massachusetts (42.6°N, 71.5°W). Earlier reports in this series have described the radar system and the means by which it can be employed to determine ionospheric densities and temperatures, and have presented the results obtained in the years 1963[1] and 1964.[2] Shorter versions of these reports, presenting for each year only results for one winter, one summer and one equinoctial month, have been published in scientific journals.[3,4] Other papers[5-8] have discussed the significance of these measurements in relation to currently accepted theories for the behavior of the F-region, or have presented the results of special observations such as those made during an eclipse[9] or magnetically disturbed conditions.[10]

The large volume of data gathered during the synoptic measurement program precludes its complete publication in the scientific journals; hence, there is a continuing need for technical reports such as this, in which all the results may be made available. In this report, we continue the practice begun earlier of presenting our results graphically, although we recognize that many users would prefer them in tabular form. However, a single figure covering a 24-hour period can represent 24 tables, each having about 100 entries, and thereby provide an immense saving in space. Further, most users would prefer to have the graphs available, even if tables could be included. Finally, tables would not solve the major problem encountered, i.e., that of transcribing the data into a computer for analysis. The remedy presumably lies in being able to transmit the results to particular users in computer-usable form, and we are currently working toward this end.

A number of changes to the instrumentation and observing procedure, that have influenced the quality and quantity of the results, were made during 1965 and are described in Secs. II and III. Section IV is a brief review of the data-reduction procedures, while Secs. V and VI present results for electron density and ionospheric temperatures, respectively. Although the year 1965 was on the rising part of the sunspot cycle, the activity was sufficiently low that most of the data could be averaged to produce monthly means. Some data were taken during disturbed periods, however, and this is discussed in Sec. VII. Finally, Sec. VIII provides a summary and some conclusions. The report[2] containing the results obtained in 1964 included results obtained using both the UHF and L-band (steerable) radar systems. The results of the L-band observations made during 1965 have already been reported,[11] and will not be included here.

II. EQUIPMENT

A. General

The radar equipment employed in these observations has been described previously.[1] Table I summarizes the parameters of the vertically directed UHF Thomson scatter radar; these were not significantly different in 1965 than from previous years. A major change made in 1965 was the recording of signals at IF on magnetic tape for later playback and analysis. This scheme permitted a cycle of measurements to be completed in 30 minutes. To explore the spectra of the signals reflected from all the altitudes of interest without making use of this would have taken approximately 90 minutes. Since the recording system has not previously been described, we present in Sec. B below a brief outline of its functions.

While valuable in greatly increasing the amount of information that could be gathered during an observing period, the recording system proved to be one of the less reliable components of the equipment. Later (during 1966-1968) it malfunctioned in a way that was not immediately obvious, causing large amounts of data to be analyzed improperly. Fortunately, it was possible to retrieve the information by computer processing, but only at the expense of a considerable amount of extra effort. The tapes recorded during a single 48-hour run usually required 2 to $2\frac{1}{2}$ weeks to process, so that the scheme was also extremely tedious to handle.

A second major change during 1965 was the reconstruction of the spectrum analyzer to permit both halves of the signal spectrum to be analyzed. This was done in a manner which, though not recognized at the time, made it difficult to subsequently extract the parameters of electron

TABLE I

PARAMETERS OF THE UHF VERTICALLY POINTING THOMSON SCATTER RADAR

Antenna	70-m-diameter fixed parabola
Polarization	Circular
Effective aperture	1600 m^2
Frequency	440 MHz
Peak transmitter power	2.5 MW
Transmitter pulse lengths	0.1-, 0.5-, and 1.0-msec pulses used
Pulse repetition frequency	50 Hz
Receiver bandwidths	25 kHz for 0.1-msec pulses 16 kHz for 0.5- and 1.0-msec pulses 40 kHz for recording system
System temperature	~300°K (monitored continuously)
Post-detector integration	~20 dB

and ion temperatures from the spectra. For this reason and since the difficulty has some bearing on the results, we describe this change here also.

B. The Recording System

The receiver employed in the Millstone Hill ionospheric radar[1] is a multiple superheterodyne in which the signals are converted in frequency to be centered at 200 kHz. At this point, three separate outputs were made available for (1) computer sampling and integration, (2) the spectrum analyzer, and (3) the recorder. In order to record the signals at IF, we employed a 1.5-MHz bandwidth tape recorder (MINCOM type CM107). When operated at 30 ips, this recorder provided a bandwidth of 250 kHz, and permitted us to record an hour's data (i.e., two complete cycles) on a $10\frac{1}{2}$-inch standard reel of $\frac{1}{2}$-inch tape (3M-981).

Figure 1 is a block diagram of the recording arrangement. A carefully constructed 40-kHz bandwidth, 7-pole filter was employed to band-limit the recorded signals. This filter provided a response flat to within ±1 dB over the required band, and a rapid falloff thereafter. In addition to the wanted IF signals, we also recorded (1) a 100-kHz sine-wave reference tone, (2) sync pulses coincident with the leading edge of each transmitter pulse, (3) WWV timing signals, (4) voice announcements for identification purposes, and (5) start/stop signals. As the recorder had seven separate channels, the IF and 100-kHz reference signals were each recorded on two channels to provide some redundancy in the event of a poor recording.

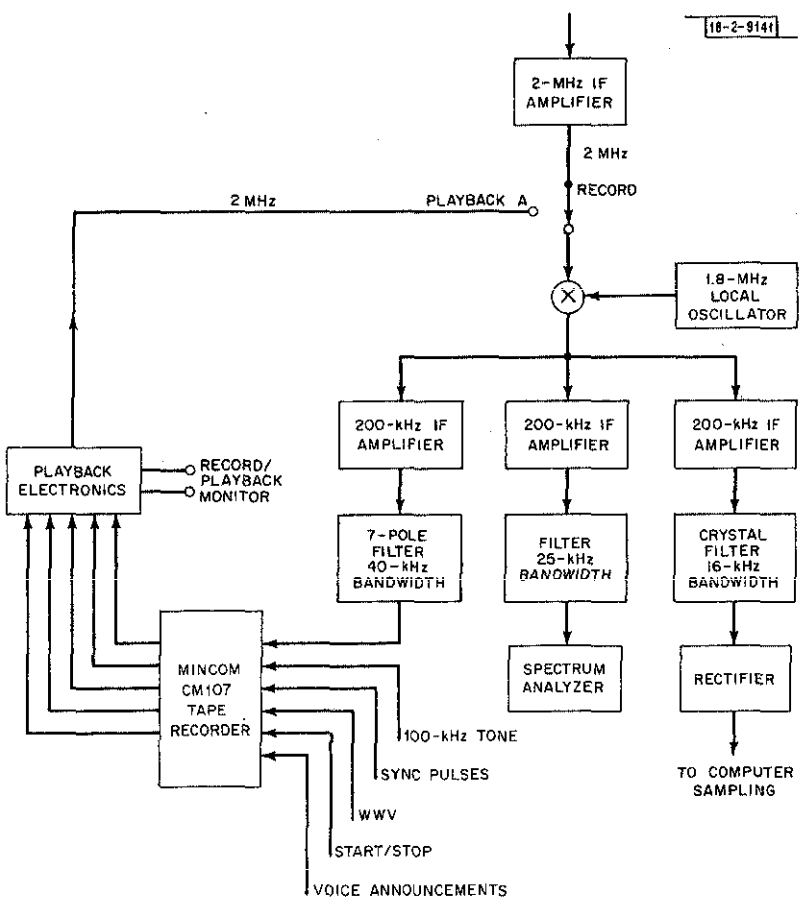

Fig. 1. Block diagram of receiver output arrangements for UHF Thomson scatter radar recording system. IF signals were recorded on magnetic tape for later spectral analysis (carried out with switch in position A).

The tape recorder was started about 20 sec prior to the beginning of a run (which always commenced on a minute mark), and a 60-Hz tone marked this interval. After a prescribed number of minutes (usually 7), the recorder was stopped. The 60-Hz tone marks thus separated each run and were used on playback to halt the tape at the beginning of a run. This "search" feature could be activated for both forward and reverse directions of the tape, thus making it relatively easy to play over a given run several times in order to analyze the spectra of the signals from different altitudes. The sync pulses recovered from the tapes were used to control a timing generator that governed the portion of the timebase being examined by the spectrum analyzer. This timing generator counted 10-μsec pulses derived from the recorded 100-kHz tone.

The tape recorder included a servo-controlled governor that could hold the tape speed constant for the full length of a recording by monitoring a 17-kHz reference tone. This feature was not utilized in our work because, for our purposes, it did not reduce sufficiently the short-period fluctuations in the recorder speed. Instead, we used the 100-kHz reference tone to synthesize a local oscillator (LO) frequency at 1.8 MHz as shown in Fig. 2. Changes in tape speed introduced frequency changes in this LO signal that were equal in magnitude but opposite in sign to those in the IF signals. Thus, by mixing the two, a new IF signal centered at 2 MHz was obtained whose frequency was independent of fluctuations in tape speed. This 2-MHz signal was then applied to the spectrum analyzer by throwing the switch to position A in Fig. 2. The recovered 2-MHz IF signal was band-limited by a 7-pole, 100-kHz wide filter which rejected spurious frequencies.

Two difficulties were encountered with the scheme of Fig. 2. The first was that "dropout" of the 100-kHz tone caused the loss of timing pulses as well as (less seriously) that of the 1.8-MHz LO. To minimize this problem, the 100-kHz signal was severely amplitude-limited, and then used to drive a narrow-band 100-kHz tuned amplifier. A second problem was encountered in

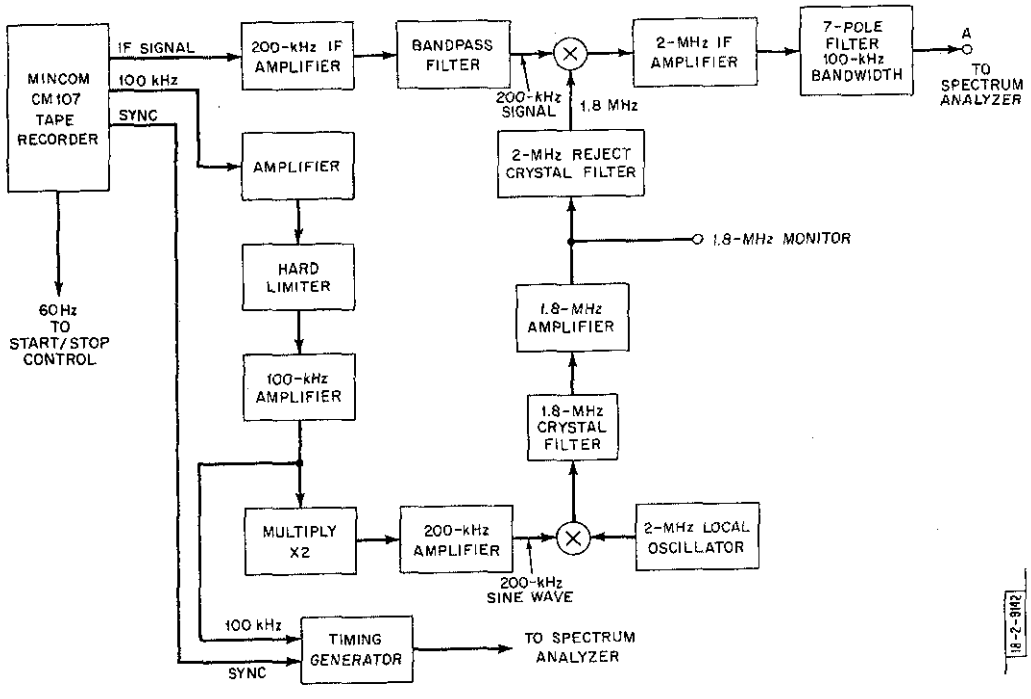

Fig. 2. Block diagram of system employed to recover IF signals from magnetic-tape recordings in a manner that eliminated undesirable frequency fluctuations introduced by changes in tape speed.

obtaining adequate spectral purity for the derived 1.8-MHz LO signal. If either 200 kHz or 2 MHz are present at the input to the signal mixer (Fig. 2), a CW signal at 2 MHz will appear at the output. This will produce a spurious level at the center of the spectrum. Adequate filtering of the 1.8-MHz signal initially solved the problem, but owing either to aging of the 1.8-MHz crystal filter or to a gradual systematic shift in the mean speed of the tape recorder, the spectral purity of the 1.8-MHz LO signal deteriorated during 1966, introducing erroneous results for the echo power at the center frequency. The single mixers shown in Fig. 2 were replaced in 1968 with balanced mixers that largely obviated this difficulty.

C. Spectrum Analyzer System

The spectrum analyzer employed in 1964[1] consisted of a bank of 24 single-pole crystal filters and 48 DC (Miller) integrators arranged as shown in Fig. 3. The filters were 500 Hz in bandwidth and spanned an 11-kHz window that could be moved to cover either the upper or lower sideband of the signal spectrum. The rectified outputs of these filters were connected to one of two integrators via high-speed switches S_1 to S_{24}.

On each sweep of the timebase, the IF signals were applied to the filters for a period equal to the length of the transmitted pulse (0.5 or 1.0 msec) at a delay following the transmitted pulse that defined the height of interest. The resulting signal voltages (together with noise) at the filter outputs were summed and stored in the odd-numbered integrators 1 through 47. The switches S_1 to S_{24} were then thrown and a second pulse of equal length applied to the gated amplifier at a point near the end of the sweep. This caused a sample of noise to be applied to the filters and the voltages to be stored in the even-numbered integrators. At the end of the integration period (typically 6 minutes), the gate pulses were removed to stop the integration process, and the voltages at the integrator outputs were automatically measured and recorded on punched-paper tape.

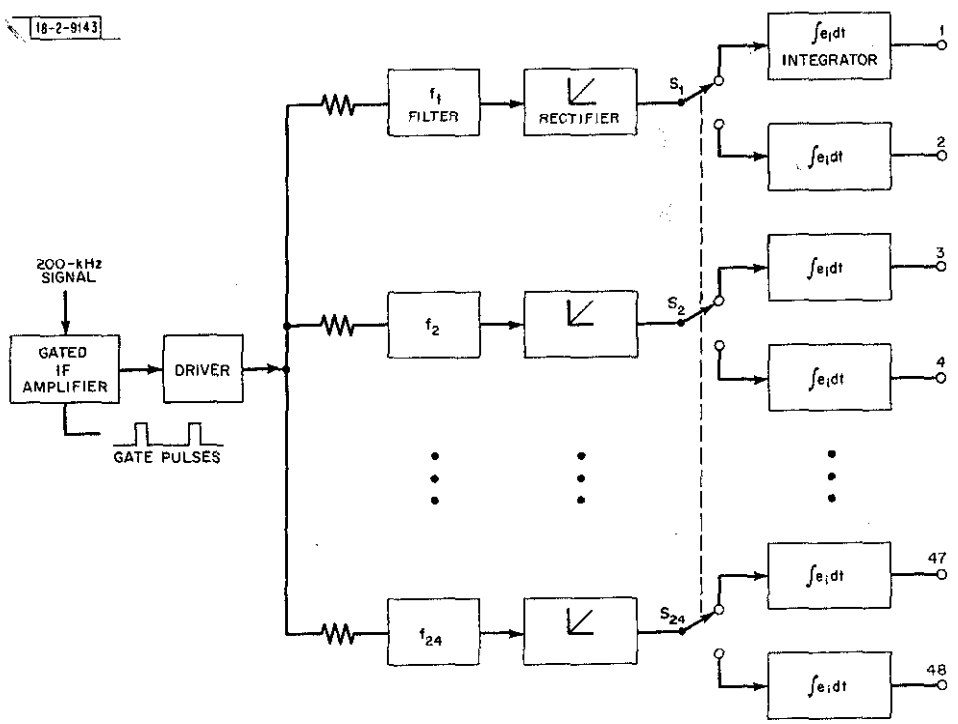

Fig. 3. Block diagram of spectrum analyzer employed from January 1963 through June 1965.

The punched-paper tape was later analyzed using a digital computer which squared the measured voltages and obtained the signal-to-noise ratio at each frequency as

$$\frac{P_s}{P_n} = \frac{(\overline{V}_{s+n})^2}{(\overline{V}_n)^2} - 1 \qquad (1)$$

where $\overline{V}_{s+n}$ is the mean voltage due to the first pulse and $\overline{V}_n$ that due to the second. This procedure eliminated the undesirable systematic errors introduced in the shape of the measured spectrum by the overall bandpass response of the receiver, or differences in the gains of the filter/rectifier combinations. However, systematic differences in the gains of the even and odd integrators in each pair were not removed, so that calibration runs were necessary. These runs were carried out by moving the first pulse out to a delay where only noise would be present, and by recording noise voltages in both sets of integrators. The computer determined a running weighted average of a number of such measurements in order to correct each signal spectrum. We also thought it necessary to correct for DC drifts in the integrators and this was done by removing the signals and allowing the integrators to drift for a time equal to the normal integration time. We later averaged all such drift measurements using the computer to obtain a set of voltage corrections to be applied to all the other measurements.

We normally employed the system described here to examine only the upper half of the signal spectrum. If an asymmetry were present, we thought it would be removed by the synchronously pumped electron-beam parametric amplifier (employed as first amplifier in the receiver), since this caused the signals to be folded about the radar frequency. Tests to examine the lower half of the spectrum, made early in 1965, disclosed a systematic difference between the two halves. We now believe this was caused by the asymmetry of the response of the filters about their center frequencies. At the time, however, this was not certain and, believing that the effect was of instrumental origin, we began to measure both halves of the spectrum and average the results. This change doubled the time required to analyze the magnetic tapes of the IF signals, and prompted the search for a modification to the spectrum analyzer that would permit both halves to be measured simultaneously.

We did not consider it desirable to distribute the 24 filters across the full 22-kHz window to be examined because, despite the precautions outlined above, instrumental effects remained the predominant source of inaccuracy. Accordingly, we decided to employ 48 filters and use the available 48 integrators to store only the difference between the signal and the noise. The scheme we developed for this is shown in Fig. 4.

In the modified spectrum analyzer, the filter outputs were rectified by a pair of full-wave rectifiers providing voltages of opposite polarity. These rectifiers were made nearly identical by employing the same transformer to drive both sets of diode rectifiers. The original high-speed switches (Fig. 3) were replaced by mercury relays (S_1 to S_{48}) that switched each integrator between these oppositely polarized rectifiers. In this manner, the noise voltage due to the second pulse was automatically subtracted from the signal-plus-noise produced by the first pulse. Systematic differences between these rectifiers were treated as DC drifts, i.e., the drift measurement was now performed with two noise pulses applied to the filters per sweep.

The scheme shown in Fig. 4 is not immune from errors introduced by channel-to-channel gain differences, and, to remove these, we performed separate calibration runs in which only the second (noise) pulse was applied to the filters on each sweep. Again, a running weighted

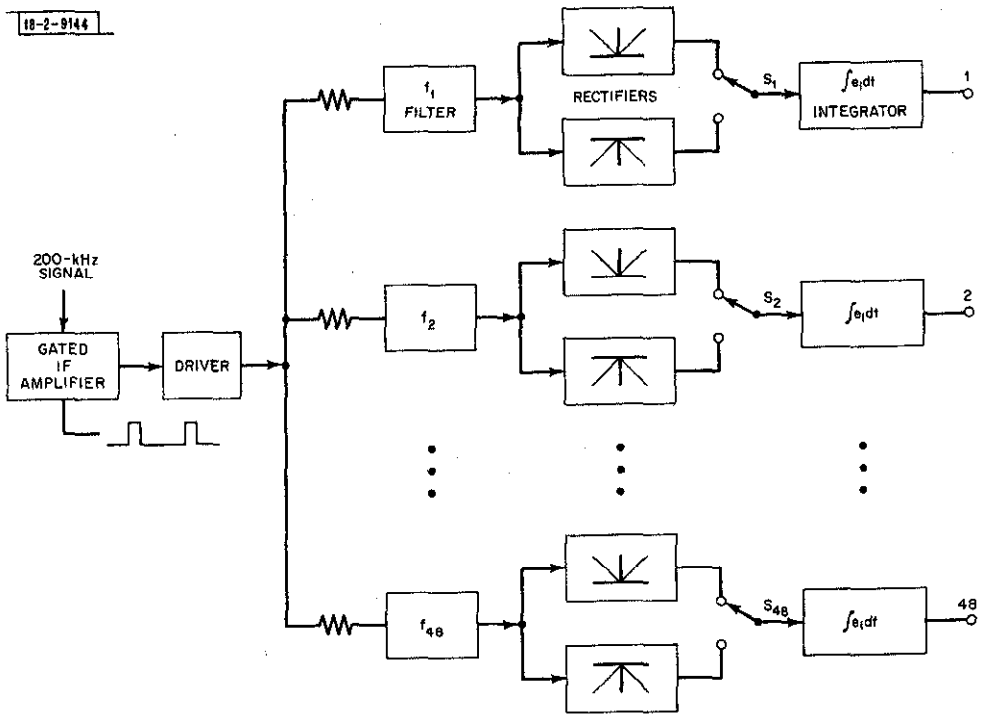

Fig. 4. Block diagram of spectrum analyzer employed from July 1965 through June 1968.

average of these calibration runs was obtained by the computer to correct each signal measurement. Instrumental errors in this scheme were probably lower than those of the original system because the automatic noise subtraction eliminated the need for two identical integrators. The changeover from the original to the modified spectrum analyzer was made prior to the July 1965 observations, and no further major changes were made until July 1968 when an entirely new system was brought into operation.

A major disadvantage of the modified system, not recognized at the time the change was made, is the difficulty of deciding the relationship between the measured voltages and the required power spectrum. Where the signal-to-noise ratio is strong $[(P_s/P_n) \gg 1]$, the measured signal voltage $\overline{V}_s$ will be much larger than the noise so that

$$\frac{P_s}{P_n} \propto (\overline{V}_s)^2 \quad . \tag{2}$$

On the other hand, when the signal-to-noise ratio is small $[(P_s/P_n) \ll 1]$

$$\frac{P_s}{P_n} \propto \overline{V}_s \tag{3}$$

implying that for small signals the rectifier behaves as a square-law device. Figure 5 shows the transition between these two regimes. The consequences of this behavior on processing the results are discussed in Sec. IV-C.

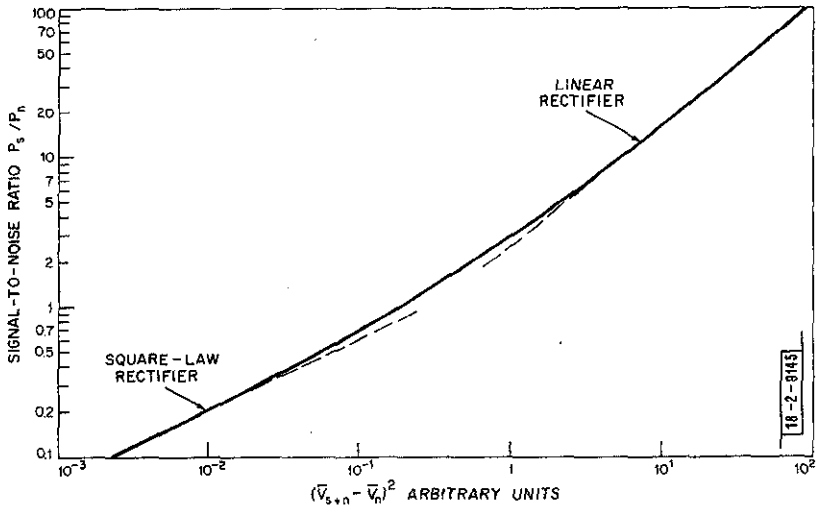

Fig. 5. *Square of voltage (abscissa) measured by spectrum analyzer shown in Fig. 4 vs input signal-to-noise ratio. For weak signals, stored voltage was directly proportional to signal power.*

III. OBSERVATIONS

During 1963, observations were made for 30-hour periods approximately four times per calendar month.[1] A complete observing cycle required 90 minutes. This was reduced to 1 hour in 1964[2] and, as a result, fewer observations were made per month as shown in Table II. By recording the IF signals for later processing, the time to obtain a complete temperature and density profile was further reduced in 1965 to 30 minutes. The impetus for these changes was our desire to better follow the behavior through dawn and dusk. As a result of this increase in the time resolution, we chose to observe over a single 48-hour period in each month. We generally chose these periods to include the Priority or Quarterly International Geophysical World Days occurring near the middle of each month. Table III summarizes the days on which measurements were made, and the mean of the planetary magnetic index K_p during these periods.

For the majority of the observing periods, the average K_p index was less than 2_o, indicating the absence of major activity and permitting the results to be averaged to obtain the mean monthly behavior with some confidence. Indeed, from an examination of the data it was evident that only in the case of June was this not permissible. The effects of magnetic disturbances on the results are discussed in Sec. VII.

TABLE II

OBSERVING PROGRAM AS A FUNCTION OF YEAR

Year	Length of Each Observing Period (hours)	No. of Observing Periods per Month	Time Taken to Measure One Profile (hours)	No. of Profiles Obtained per Month
1963	30	4	1.5	80
1964	30	2	1.0	60
1965	48	1	0.5	96

TABLE III

INCOHERENT SCATTER OBSERVATIONS – 1965

Begin (EST)			End (EST)			Mean K_p	Comment
12 January	D	1100	14 January		0700	2+	Somewhat disturbed
16 February		1000	18 February	q	0700	1–	Quiet
6 April		1300	8 April	Q	1100	1+	Quiet
13 April		0900	15 April	q	0900	1_o	Quiet
18 May		0800	20 May		0800	1–	Quiet
15 June	D	1100	16 June	D	2100	5+	Very disturbed
20 July		0800	22 July		0800	1_o	Quiet
17 August		0800	19 August	D	0800	3–	Somewhat disturbed
14 September	Q	1100	16 September	D	1100	3_o	Somewhat disturbed
26 October		0800	28 October	D	0800	2–	
16 November	Q	0900	18 November		0800	1_o	Quiet
21 December	Q	1300	23 December	q	1200	1_o	Quiet

IV. DATA REDUCTION

A. F-Region Critical Frequency

The incoherent scatter results obtained at Millstone are employed to derive only the shape of the electron-density-vs-height profile. The absolute density values are established by assigning a value to the peak density of

$$N_{max} = 1.24 \times 10^4 (f_o F2)^2 \text{ electrons/cm}^3 \quad (4)$$

where $f_o F2$ is the F-layer critical frequency observed on an ionosonde. Previous examinations of the critical frequency measured using the Millstone Hill C-4 ionosonde with measurements made at Fort Belvoir, Virginia (38°N, 77°W) have indicated good correspondence between the two. Owing to equipment malfunctions, good records were not always obtained at Millstone; hence, in computing N_{max}, we chose to employ the Fort Belvoir values of $f_o F2$.

As a first step, we plotted $f_o F2$ as a function of local time for all the hours of observation, and smooth curves were drawn through the points as shown in Figs. 6(a-l). On a number of days (e.g., 20-21 July and 17-18 August), $f_o F2$ did not repeat very well, but we did not regard the different behavior as serious, since no obvious differences could be found in the shape of the electron density profiles or the temperatures. In the case of June [Fig. 6(f)], the behavior was so different on the 15th and 16th that we made no attempt to construct an average 24-hour curve.

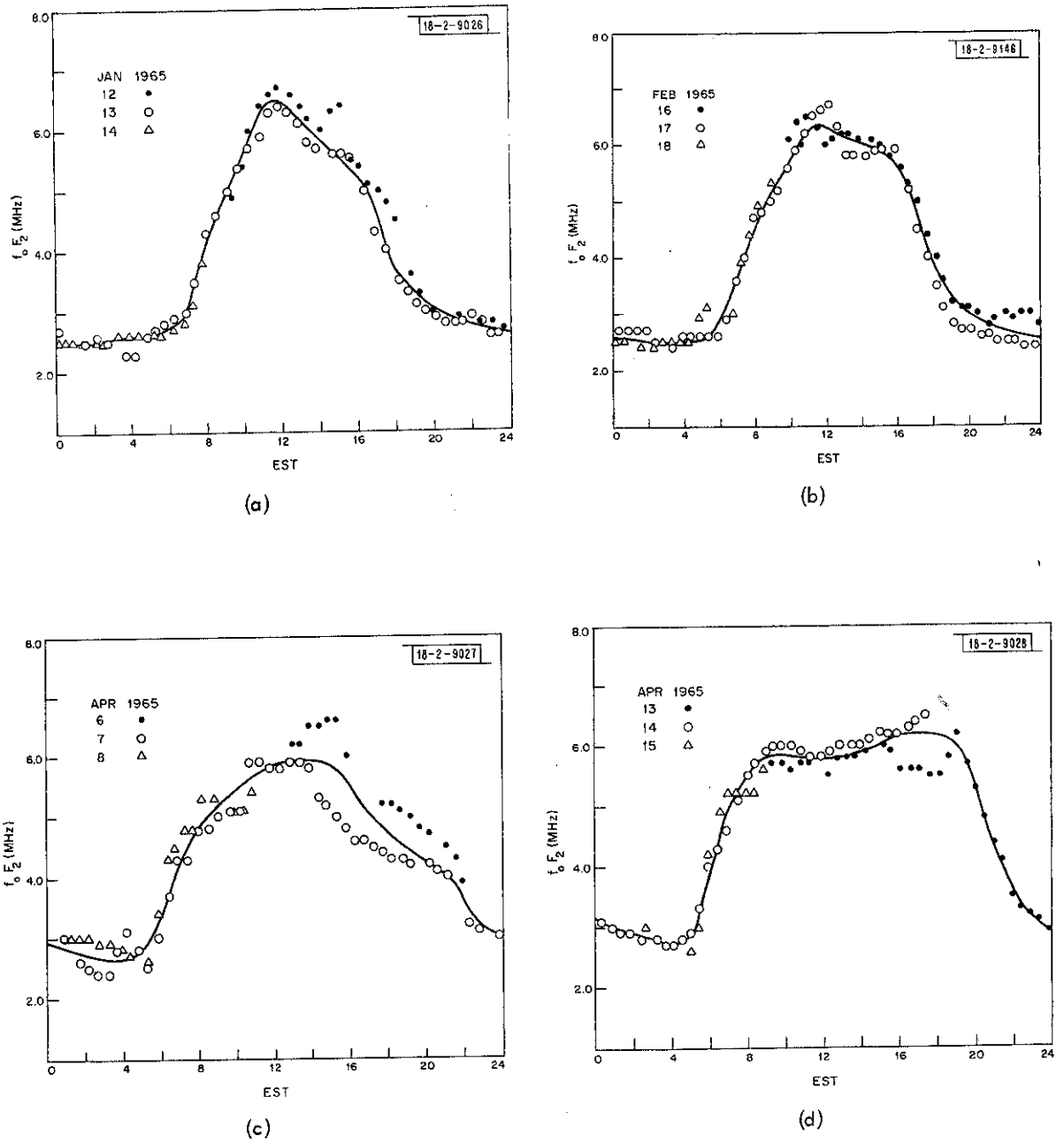

Fig. 6(a-l). F-region critical frequency vs local time for periods of observation in 1965.

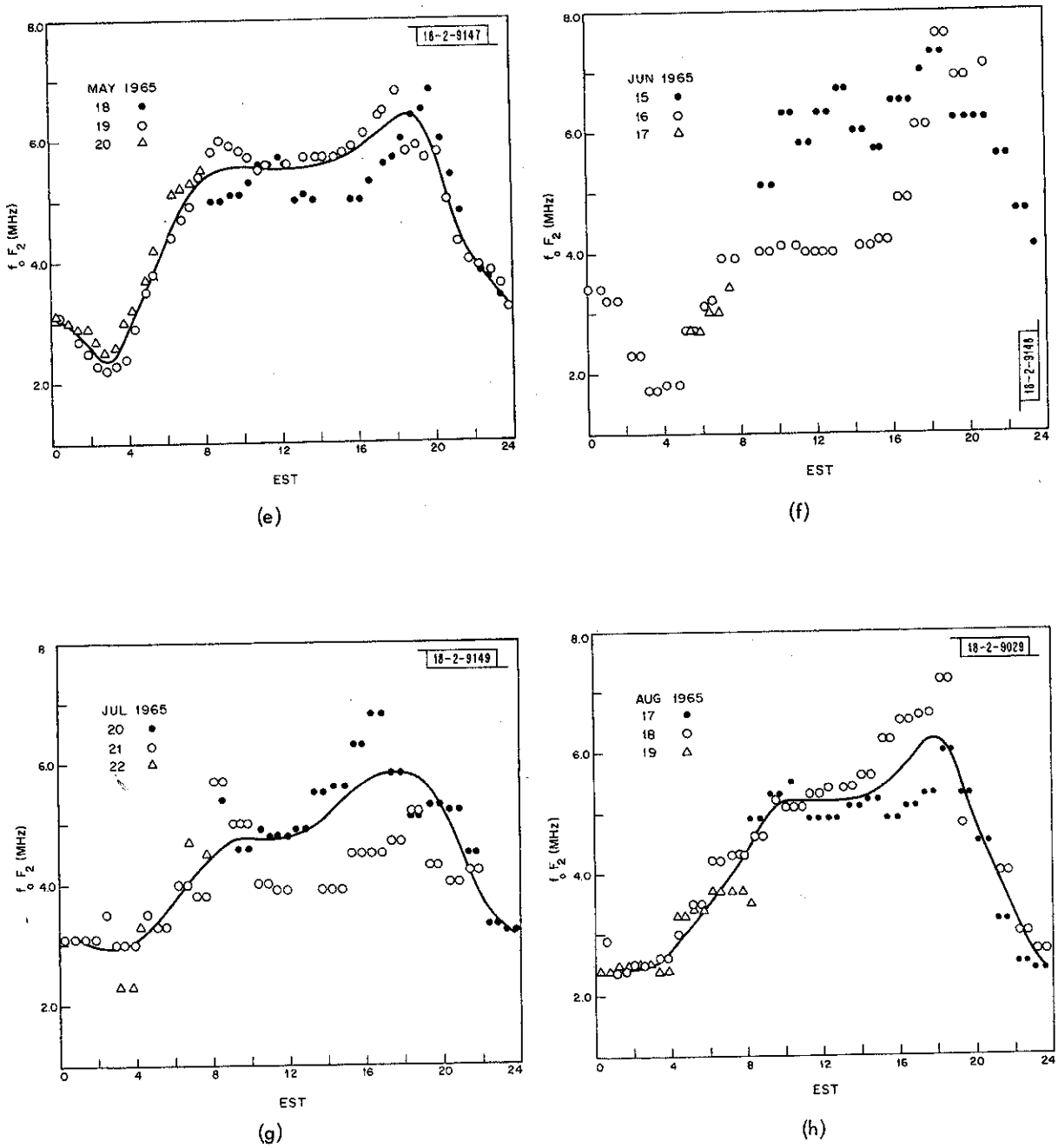

Fig. 6(a-l). Continued.

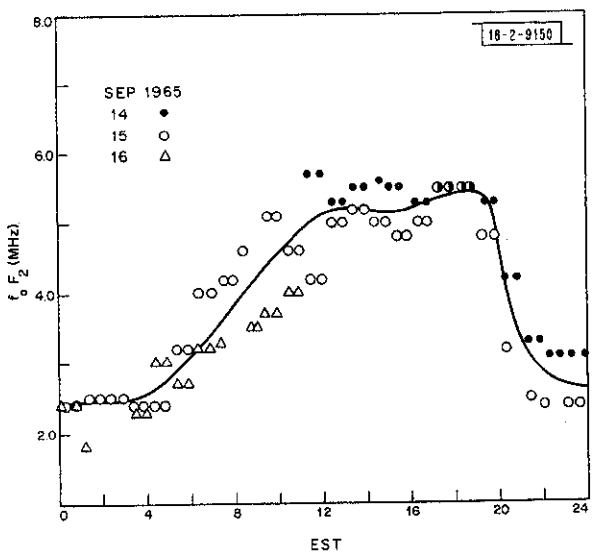

(i)

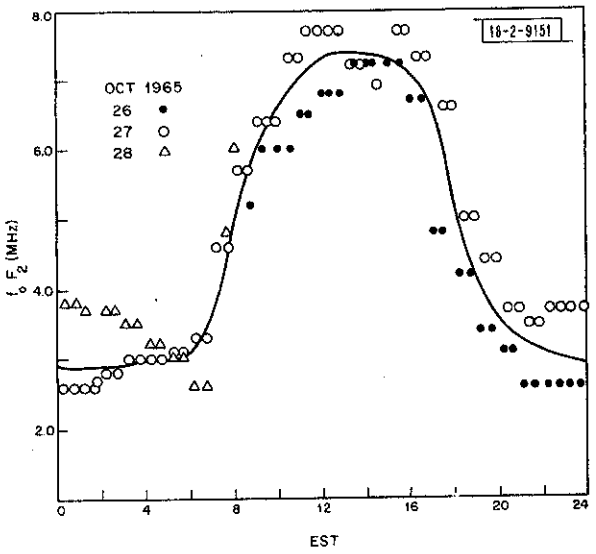

(j)

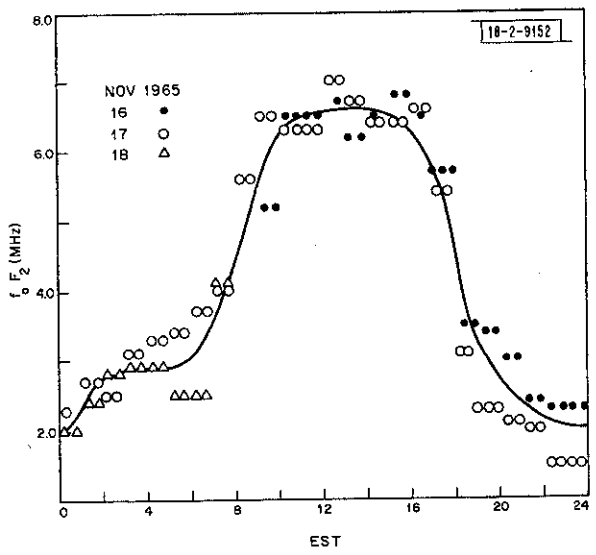

(k)

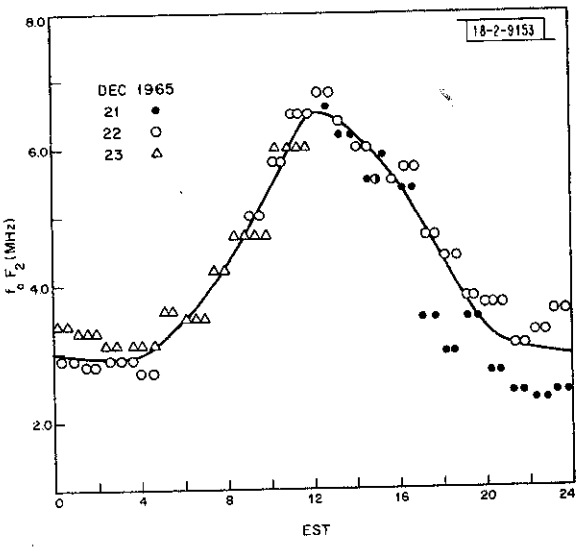

(l)

Fig. 6(a-l). Continued.

B. Electron Density Profile

Echo power vs delay observations using 0.1-, 0.5-, and 1.0-msec pulses were combined to yield an echo power profile P_s vs height h from

$$P_s(h) = \frac{T_s(h)}{h^2} \tag{5}$$

where T_s is the equivalent echo temperature observed at the completion of the sweep integration.[1] Next, these power profiles were corrected for the effect on the scattered power of the electron-to-ion-temperature ratio T'_e/T_i obtained from the analysis of the signal spectra[2]

$$N(h) \propto P_s \left[\frac{1 + (T'_e/T_i)_h}{1 + (T'_e/T_i)_{h_{max}}} \right] . \tag{6}$$

These corrected profiles were then assigned the value of the peak electron density N_{max} obtained via Eq. (4).

Although an independent electron density profile was obtained every 30 minutes, the scatter of the temperature results was so large that we were obliged to compute only the hourly averages. To do this, all the power profiles obtained in each hour were scaled at given altitudes with respect to the peak, and a mean taken to obtain a profile with the average shape. This mean profile was adjusted in height to place the peak at the mean of the peak heights, and its shape was corrected according to Eq. (6) using the hourly mean values of T'_e/T_i (Sec. C below). The peak density for these mean hourly profiles was taken to be the mean of the individual values of N_{max}.

The accuracy of this procedure has been discussed previously.[2] For the data taken since June, the accuracy probably decreased owing to systematic errors introduced in the values of T'_e/T_i (Sec. IV-D).

C. Electron and Ion Temperatures (Prior to July)

In analyzing the measurements made prior to July, we employed the same procedures used in 1964.[2] That is, the 24 points in each spectrum were machine-plotted on charts, and smooth curves were drawn through these by eye. These smooth curves were next hand-scaled to yield the parameters of <u>width</u> (to half peak power) and <u>ratio</u> (between the power at the center frequency and that in the wing). The electron and ion temperatures were then determined from the width and ratio values by interpolation using charts showing the variation of these quantities for fixed values of T_i and the ratio T'_e/T_i (Ref. 1). These charts were prepared[2] on the assumption that O^+ is the predominant ion present and that the plasma frequency everywhere is 10 MHz. This last assumption leads to the electron temperature being underestimated, and the values obtained are described as <u>fictitious</u> and are represented by the symbol T'_e.

The values of T_i and T'_e were divided into hourly groups and plotted as a function of altitude. Smooth curves were next drawn through the points and extrapolated down to a value of 355°K at 120-km altitude, i.e., the fixed temperature assumed in the CIRA 1965 model atmospheres.

The ratio T'_e/T_i scaled from these plots was employed in Eq. (6) to obtain the corrected density profiles as outlined above. These corrected profiles were then employed to convert the fictitious electron temperatures to true values via[2]

$$T_e = T'_e \left(1 - \frac{1.62T'_e}{N}\right)^{-1} . \tag{7}$$

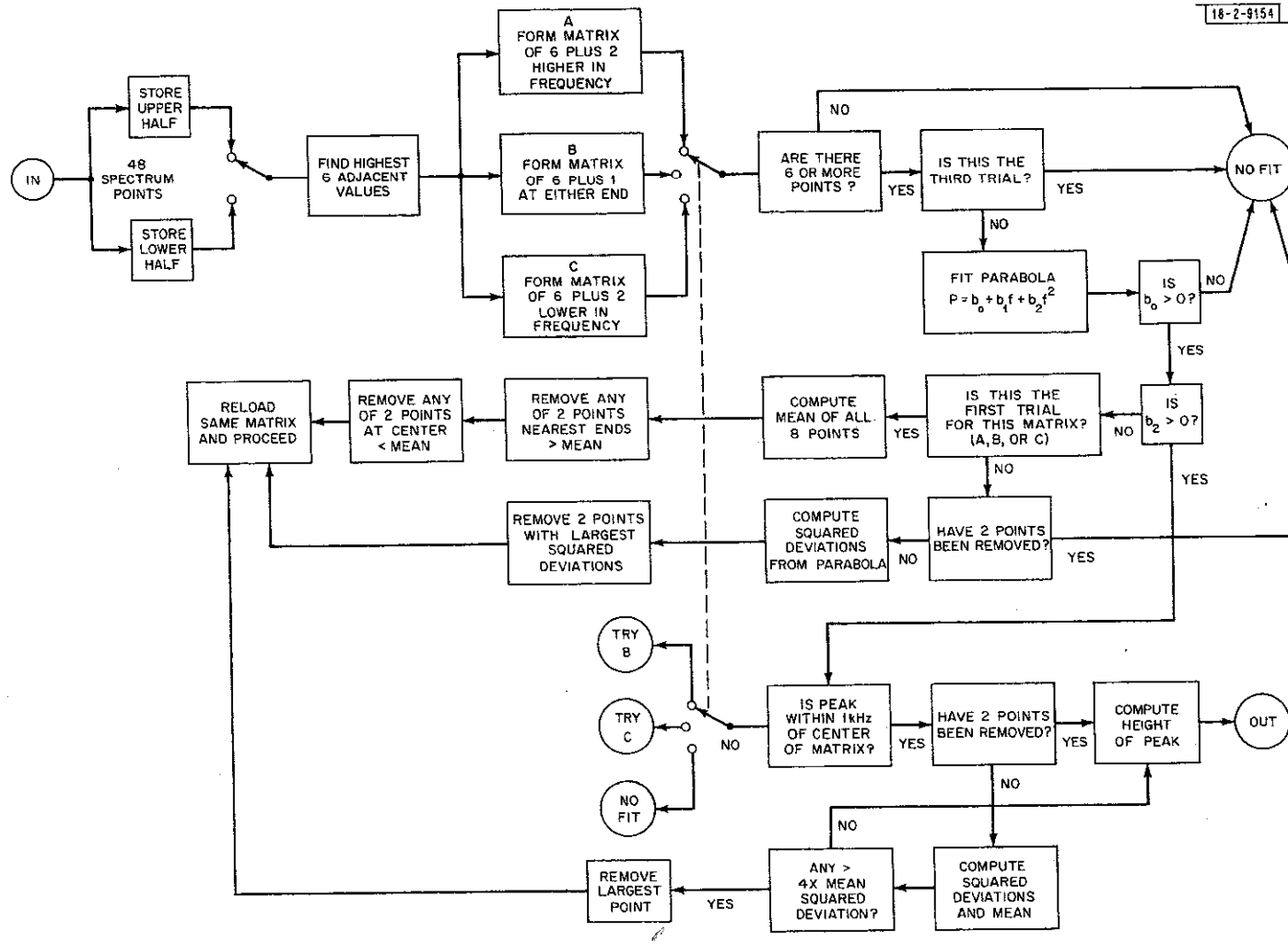

Fig. 7. Logic flow diagram of part of computer program employed to process signal spectra to obtain temperature measurements. This section was employed to fit parabola to wing of spectrum in way that would eliminate spurious points.

This expression is believed to be reasonably accurate provided $(T'_e/N) \leq 2 \times 10^{-1}$ °K cm^3, but at higher values probably causes T_e to be overestimated. In practice, this is probably important only at altitudes above about 700 km where few useful measurements were gathered.

D. Electron and Ion Temperatures (July and Later)

Spectra obtained in July and later were completely analyzed by the computer. The philosophy employed for this was basically the same as in the earlier hand analysis. Thus, the computer first estimated the parameters of width and ratio, and inserted these into analytic expressions to yield T'_e and T_i. These analytic expressions were obtained by fitting high-order polynomial expressions (10 or more terms) to the values of ratio and width computed for various values of T_i and T'_e/T_i. The conversion of the ratio and width parameters to temperature in this way was accurate to at least 1 percent, i.e., substantially better than could be achieved using the earlier graphical method.

The major difficulty encountered with machine reduction was in devising ways of rejecting spurious points. Thus, to find the height in the center or in the wing of the spectrum, a parabola was fitted to the points. A test was then made to see if any points deviated by more than a certain number of standard deviations, and all such points were rejected. The parabola was then refitted to the remaining points. Figure 7 shows in schematic form the final procedure adopted to determine the height of one of the wings in the spectrum. To locate the edges of the spectrum, a straight line was fitted to three points nearest the half-peak value. The computer program was also required to correct for drifts and channel-to-channel gain differences as outlined in Sec. II. As a result of all these requirements, the program grew in complexity, and an entirely satisfactory version was not obtained until mid-1968. Despite the delay, this program provided immense savings in time taken to obtain temperature values.

In the course of developing the computer program to determine the temperatures, we recognized the nonlinear relation between the signal voltage measured by the new spectrum analyzer and the echo power (Sec. II-C). Based upon experience with the earlier analyzer, we knew that the spectra obtained at high altitudes (using 1-msec pulses) were invariably weaker than noise, hence, the measured voltage could be taken as the best estimate of the echo power [Eq. (3)]. Conversely, at the lowest altitude examined (225 km), using 0.5-msec pulses, the signal-to-noise ratio would nearly always be greater than unity, requiring that the measured voltages be interpreted as the square root of the echo power [Eq. (2)]. At intermediate altitudes, neither assumption would be correct, and a proper interpretation of the spectrum would require some knowledge of the signal-to-noise ratio at each frequency. Since this was not available, the best that could be achieved would be to adopt some intermediate power law at these middle altitudes. Unfortunately, the height of the spectrum was not recorded on the punched-paper tape but in a separate log, hence, this could not readily be done. As the length of the pulse (0.5 or 1.0 msec) was encoded on the punched-paper tape, we chose to employ Eq. (2) to interpret the 0.5-msec measurements and Eq. (3) for the measurements made at greater altitudes with 1.0-msec pulses.

The effect of interpreting weak signals using the incorrect relation Eq. (2) will be to cause T'_e/T_i to be overestimated, and T_i to be underestimated. The error will be least in T'_e since the two effects tend to compensate one another. For strong signals interpreted using Eq. (3), T_i will be overestimated and, again, T'_e should not be greatly in error. Therefore, the effects of these assumptions on the temperature results will be chiefly to cause parts of the T_i curve to be in error. By comparing results obtained before and after July, it appears that the error is

largest in the region 300 to 500 km where T_i has been underestimated. We attempted to compensate for this when constructing the mean hourly temperature curves. These mean profiles were used to correct the electron density profiles and were themselves corrected in the same manner as the data taken prior to July.

The accuracy of the procedures employed prior to July to obtain temperatures has been discussed.[2] The largest uncertainty in the measurements was the random error associated with determining the spectrum width and shape parameters, and this could be reduced by averaging large numbers of measurements. For the measurements taken in July and later, the systematic errors (in T_i) exceeded the random errors in the altitude range 300 to 500 km; hence, we place less reliance on these measurements than on any others reported herein. Unfortunately, these uncertainties were present also in the T_e'/T_i curves used to correct the electron density profiles.

V. RESULTS FOR ELECTRON DENSITY

A. Diurnal Plots

The mean hourly electron density profiles obtained in the manner outlined in Sec. IV are presented in Figs. 8(a-l) as contours of constant electron density (actually, plasma frequency) over the height interval 150 to 650 km and 0 to 24 hours EST. The only exception to this is the month of June [Fig. 8(f)] where, owing to the markedly different behavior from day-to-day, it was necessary to plot the 48-hour period in full. Unfortunately, equipment malfunctions caused the loss of much of the last 12-hours' data during this period. To obtain this plot [Fig. 8(f)], we constructed temperature profiles averaged over intervals of 2 hours in order to reduce the uncertainty in the measurements.

B. Mean Daytime and Nighttime N(h) Profiles

For some purposes, the electron density profiles averaged over some period are of greater use than the complete time history provided by Figs. 8(a-l). Accordingly, we computed average density curves for the periods 1000 to 1500 and 2100 to 0300 EST and these are presented in Figs. 9(a-k) and 10(a-k), respectively. These averages were constructed from the hourly averages in the same manner in which the latter were themselves computed, i.e., by averaging the profile shapes and assigning these the mean values of h_{max} and N_{max}.

There is a noticeable increase in the curvature for the region above h_{max} in the daytime profiles for July onward [Figs. 9(f-k)]. We believe this to be caused by the errors in the ratio T_e'/T_i discussed earlier which, through Eq. (6), cause the density to be progressively overestimated with increasing altitude. The effect is not present at night, since then T_e'/T_i tends to be smaller and less altitude-dependent.

C. Discussion

The main features of the winter diurnal behavior observed in 1965 differ little from those of 1964. A single daytime maximum in the peak electron density is found to occur usually between 1200 and 1300 hours. Above h_{max}, however, there is evidence of a second peak occurring at sunset which is probably the winter counterpart of the marked evening increase observed in summer. Based upon the behavior observed during a solar eclipse,[10] we attribute this phenomenon to the rapid decrease in T_e occurring at sunset and the redistribution of the ionization to which this gives rise.[5] This suggestion has produced a spirited discussion in the literature that

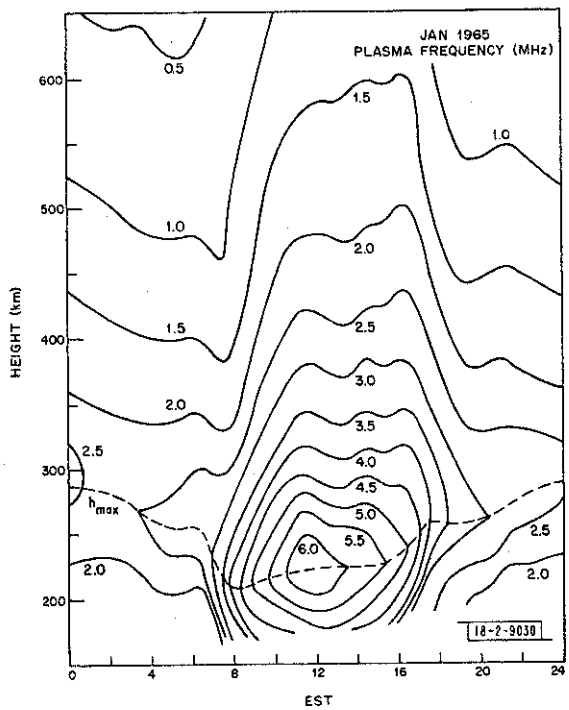

(a)

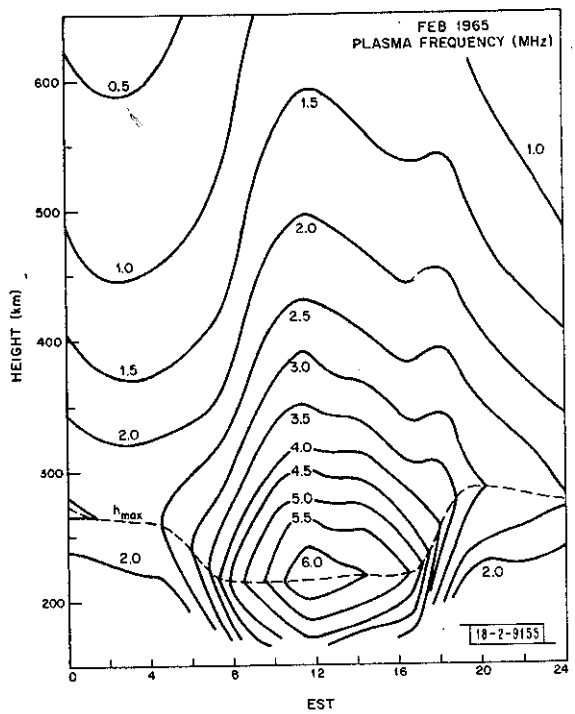

(b)

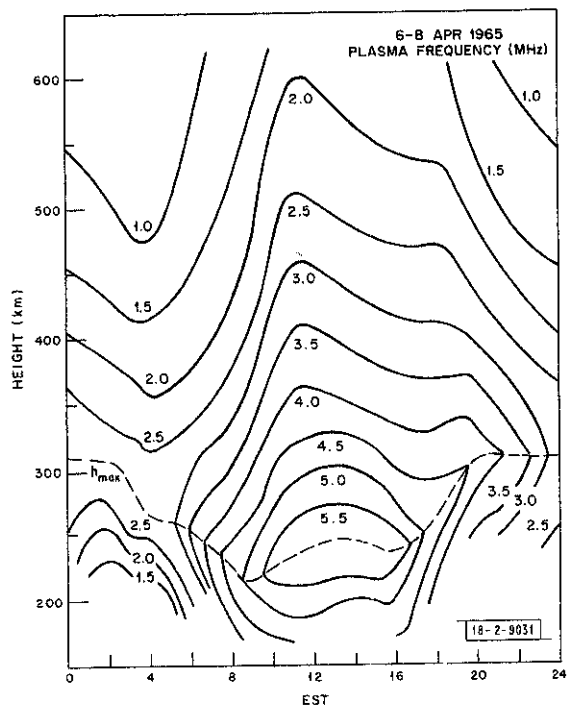

(c)

Fig. 8(a-l). Contours of constant plasma frequency observed as functions of height and local time for measurements made in 1965.

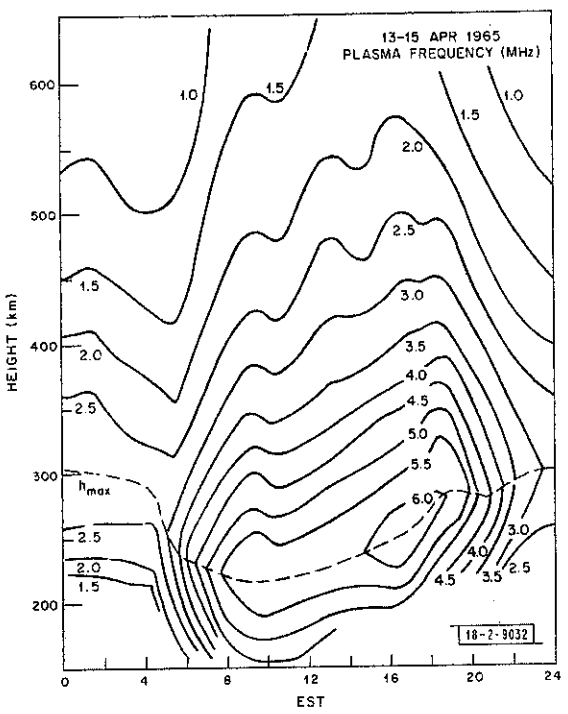

(d)

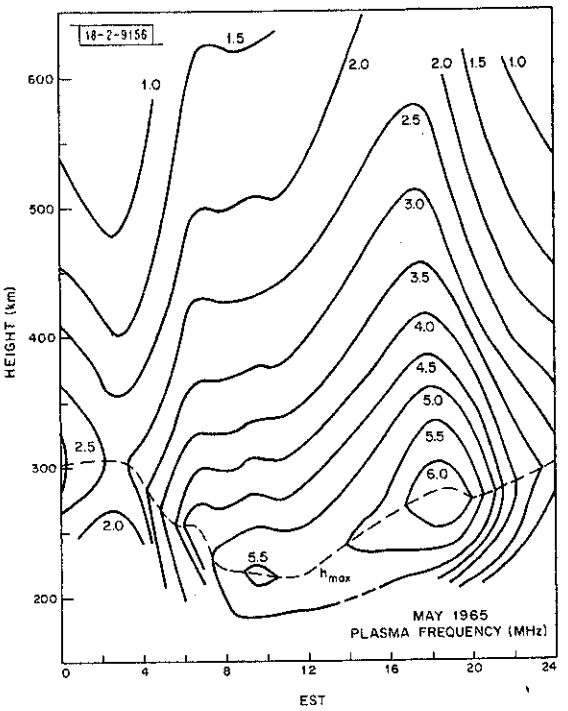

(e)

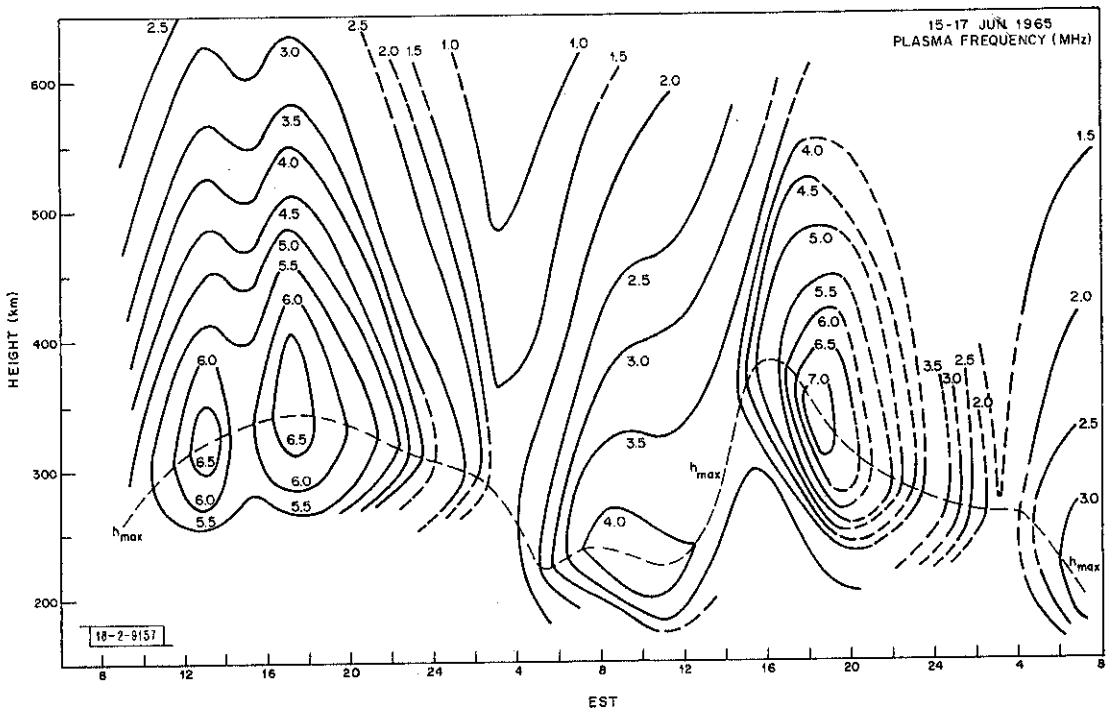

(f)

Fig. 8(a-l). Continued.

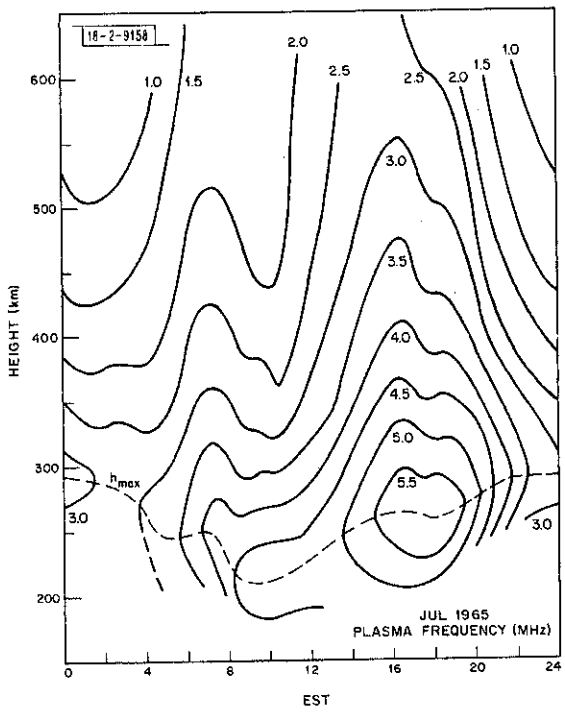

(g)

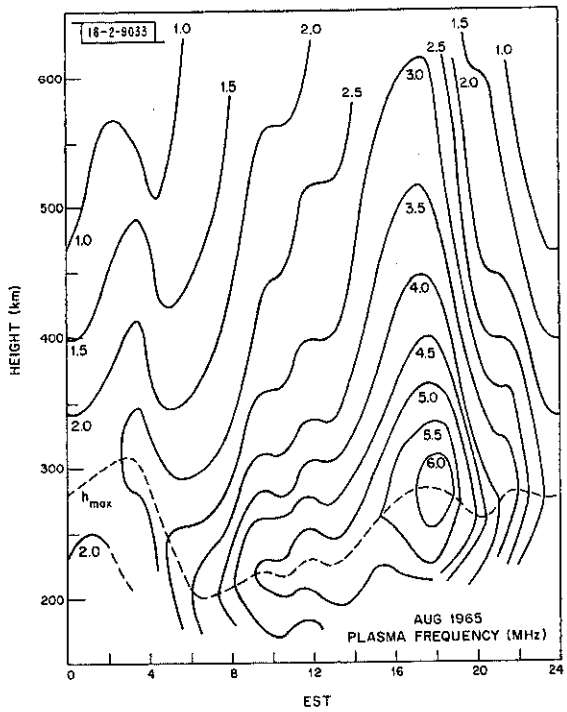

(h)

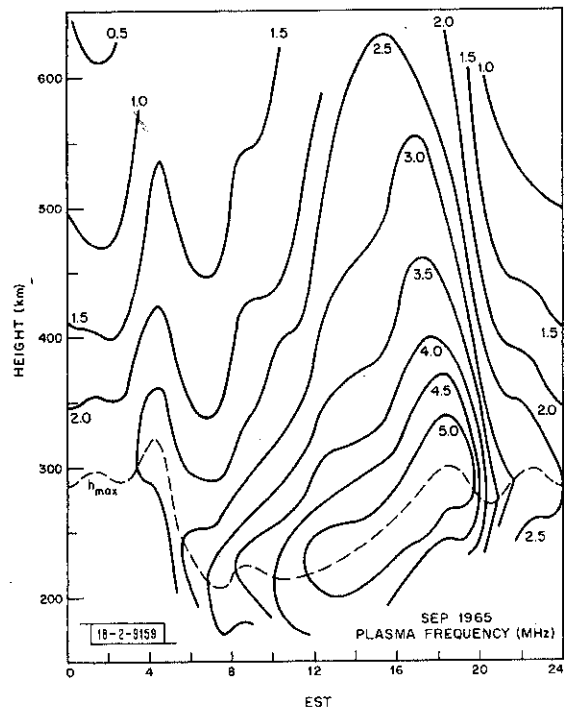

(i)

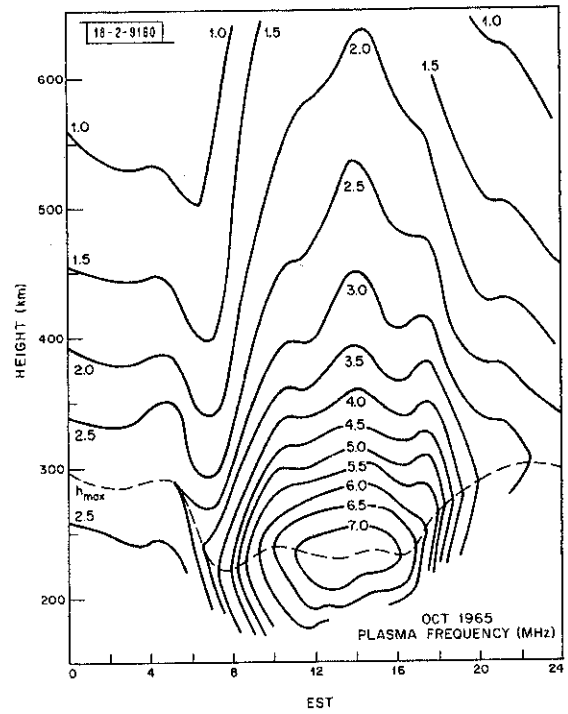

(j)

Fig. 8(a-l). Continued.

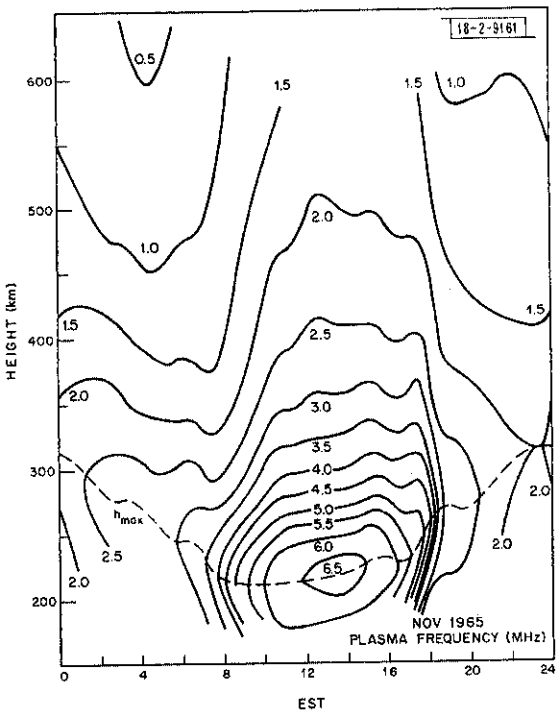

(k)

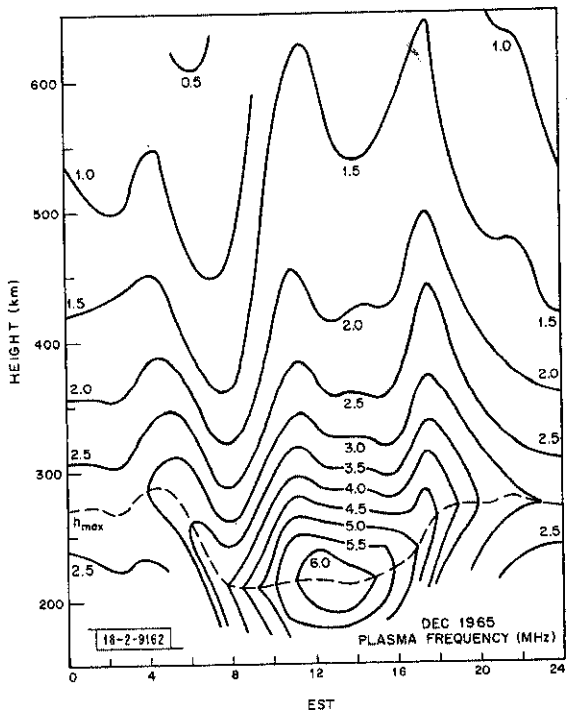

(l)

Fig. 8(a-l). Continued.

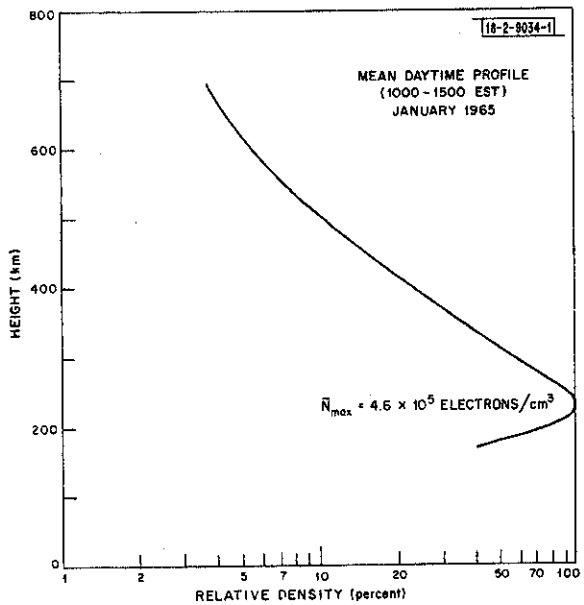

(a)

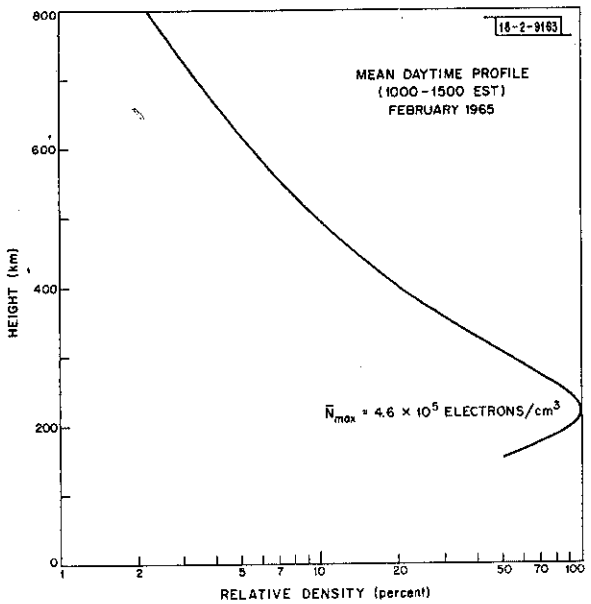

(b)

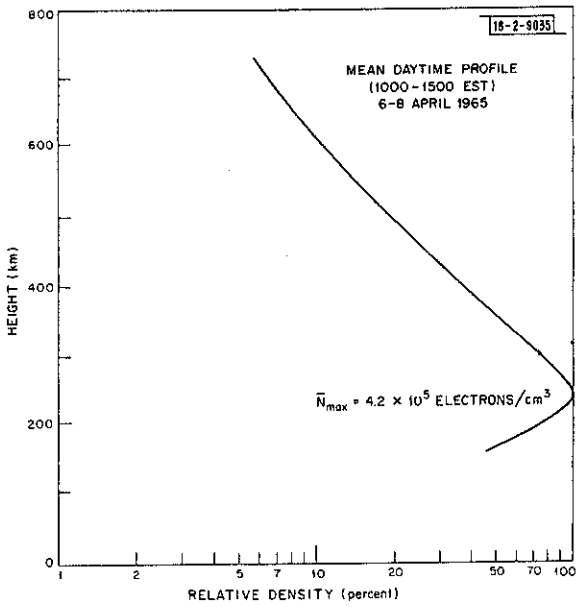

(c)

Fig. 9(a-k). Mean daytime density profiles; these plots obtained by averaging all measurements between 1000 and 1500 EST. $\bar{N}_{max}$ is mean peak density during this time period.

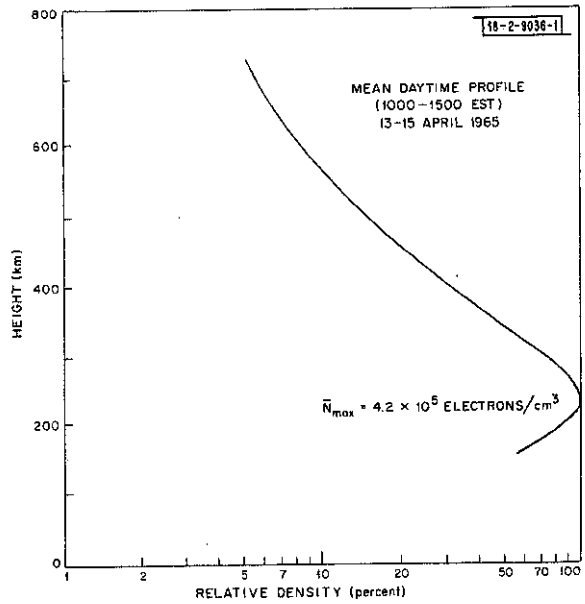

(d)

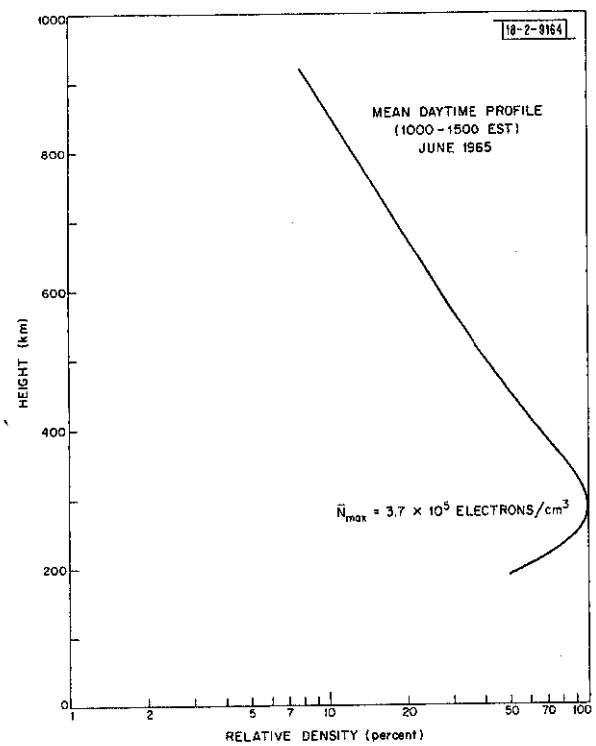

(e)

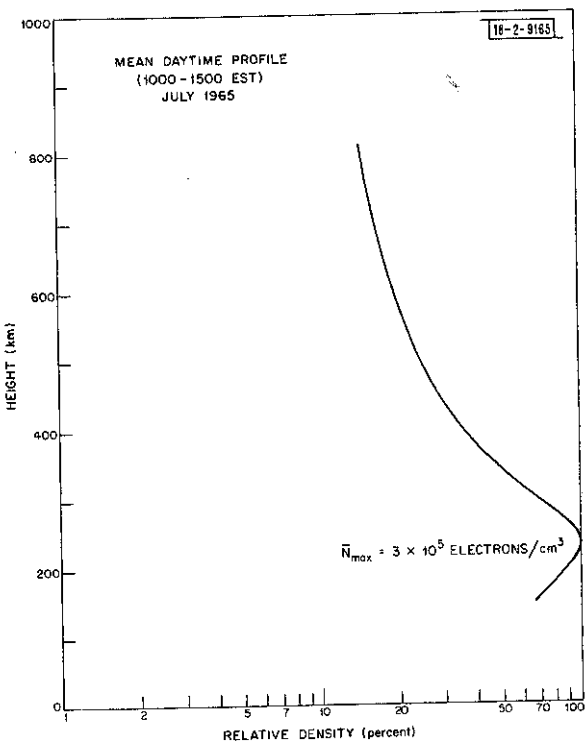

(f)

Fig. 9(a-k). Continued.

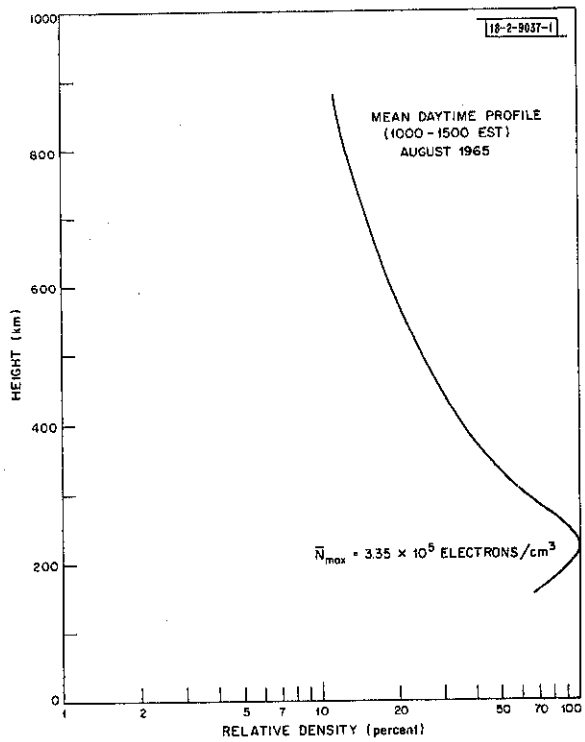

(g)

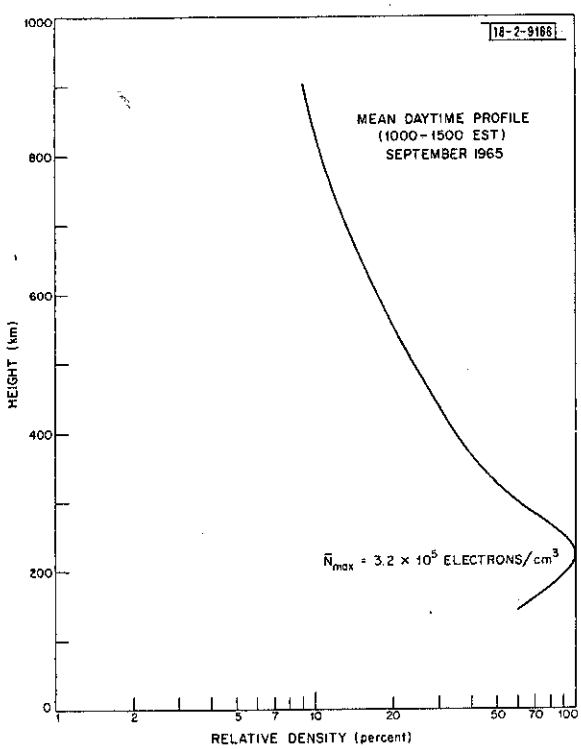

(h)

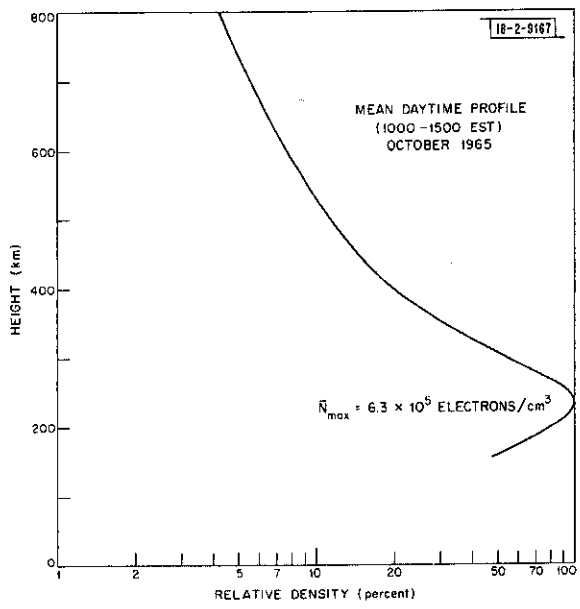

(i)

Fig. 9(a-k). Continued.

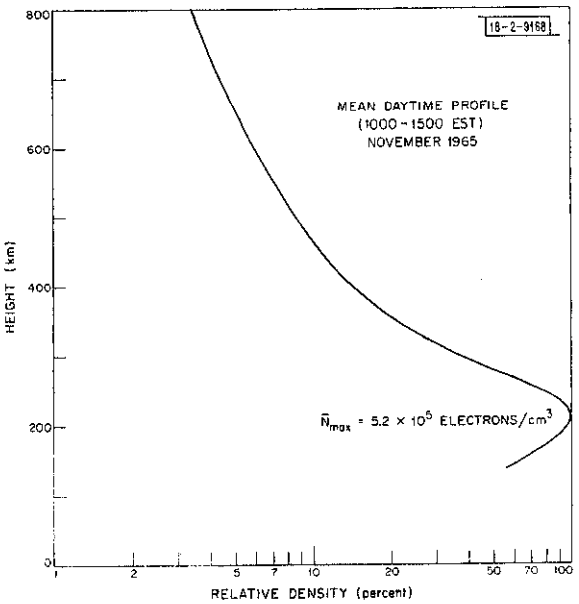

(j)

(k)

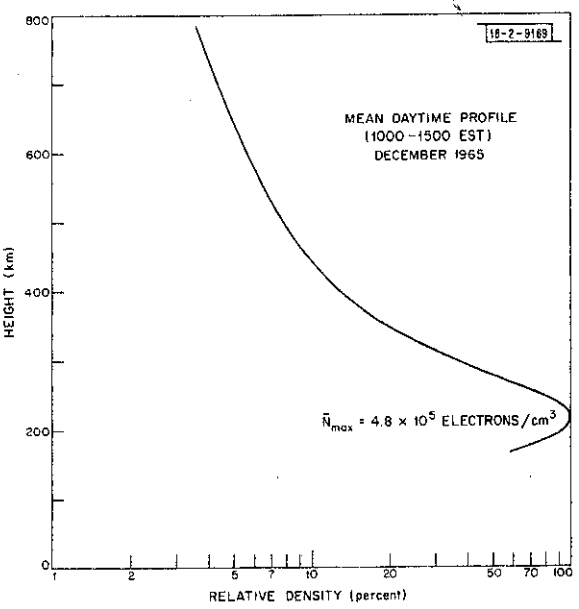

Fig. 9(a-k). Continued.

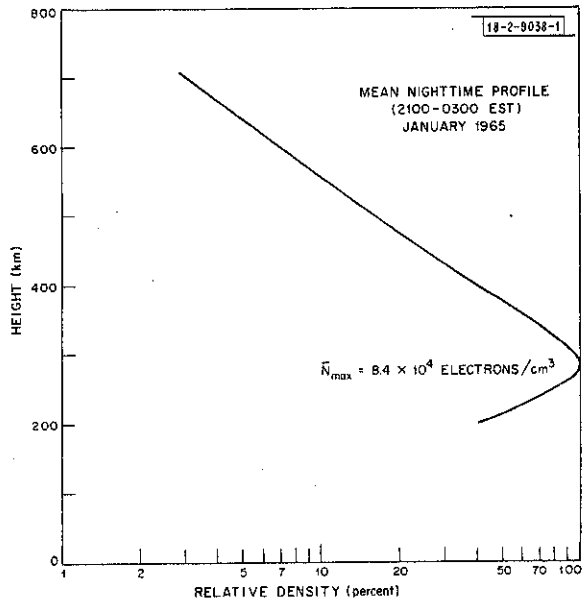

(a)

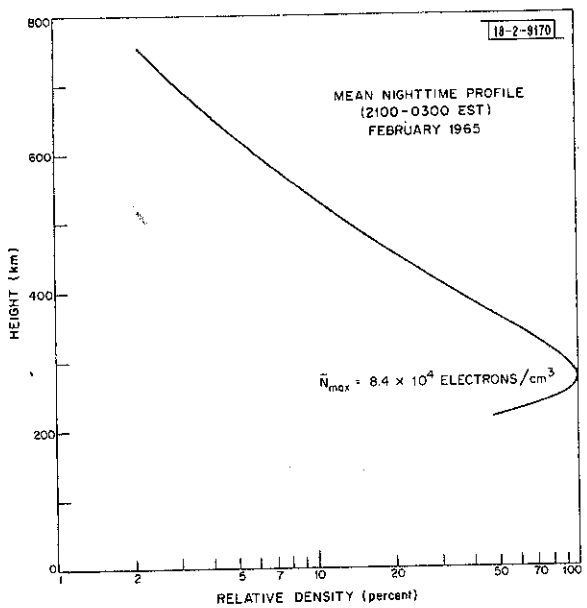

(b)

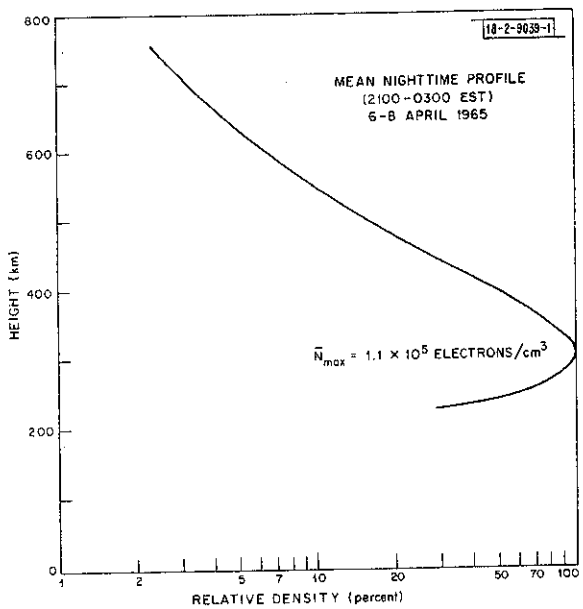

(c)

Fig. 10(a-k). Mean nighttime density profiles; these plots obtained by averaging all measurements between 2100 and 0300 EST. $\overline{N}_{max}$ is mean peak density during this time period.

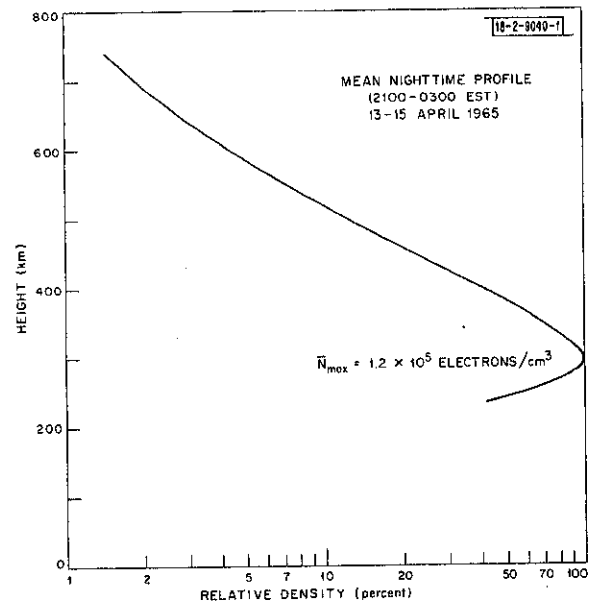

(d)

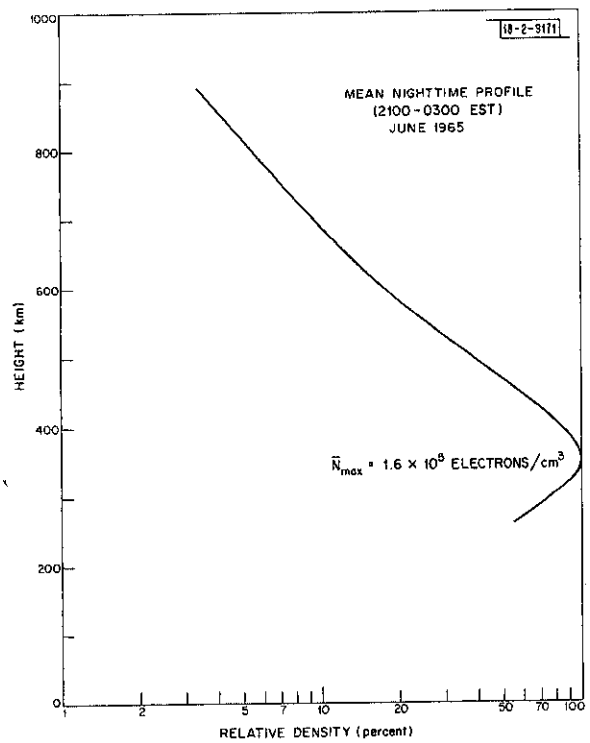

(e)

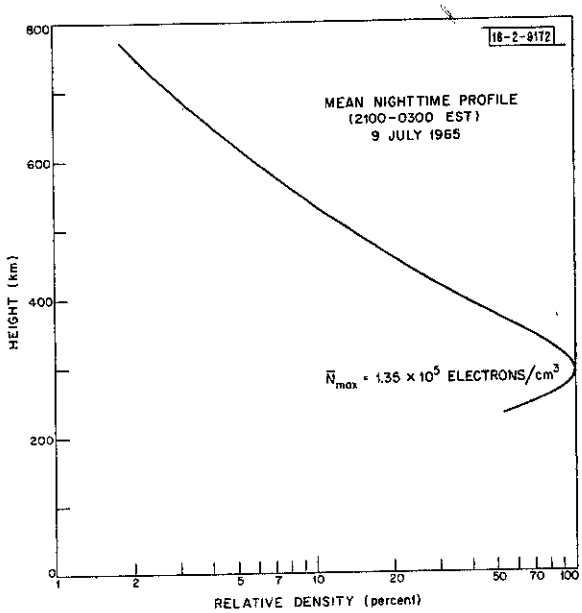

(f)

Fig. 10(a-k). Continued.

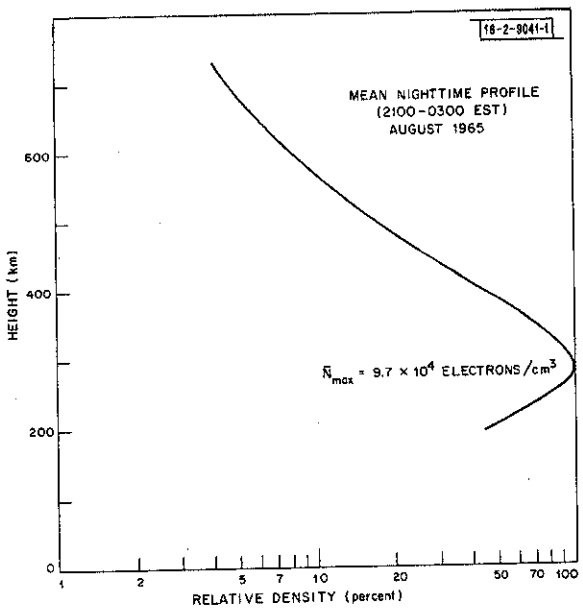

(g)

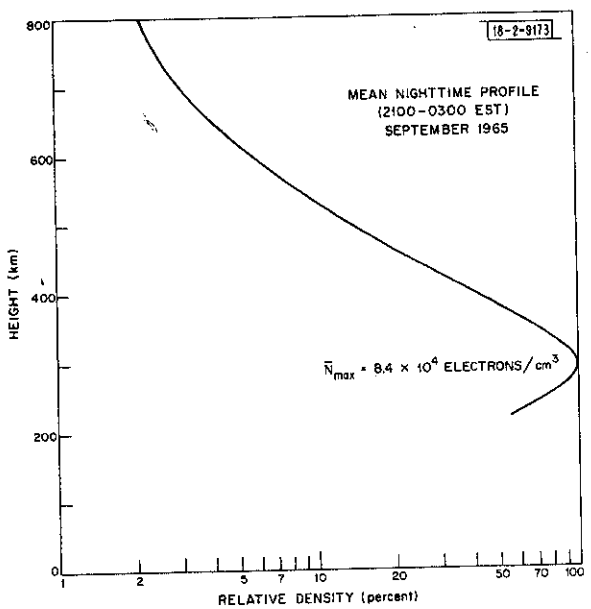

(h)

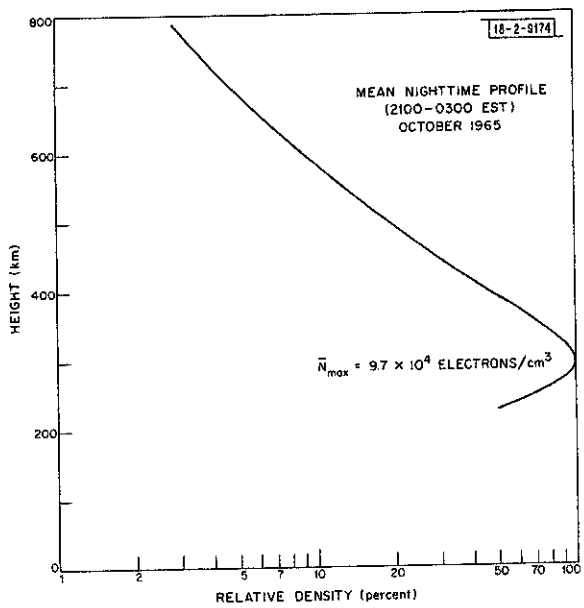

(i)

Fig. 10(a-k). Continued.

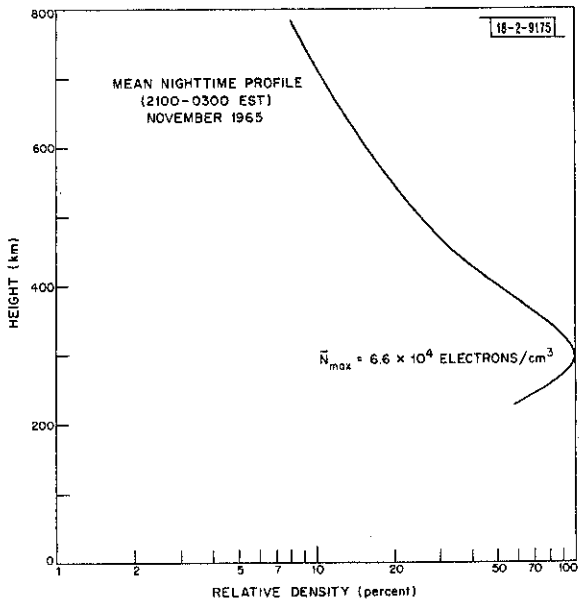

(j)

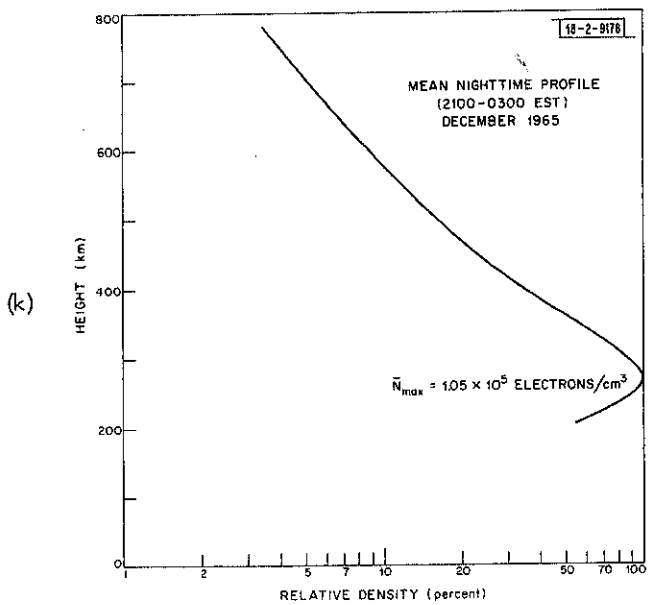

(k)

Fig. 10(a-k). Continued.

is too extensive to review here. However, we may summarize the salient points as follows. An attempt to model the phenomenon using a time-dependent solution to the electron density continuity equation has been performed by Thomas and Venables[12] employing a simple model for the electron and ion temperatures based upon the Millstone observations. This model failed to reproduce the evening increase, but a later model in which the electron temperature was allowed to govern the loss rate according to the laboratory results of Schmeltekopf, et al.,[13] did produce an evening maximum.[14]

Kohl and King,[15] and Kohl, et al.,[16] have argued that neutral winds, which serve to drive ionization down the field lines during the daytime and thereby depress the midday electron densities, are set up in the upper atmosphere. The evening maximum results from a reversal in the wind direction, which causes the ionization to be driven up the field lines to regions of lower recombination rate. The general variation of h_{max} seen in Figs. 8(a-l) supports this idea.

The most comprehensive treatment of the problem seems to have been carried out by Strobel[17] and Sterling, et al.,[18] who solved the time-dependent continuity equation including the effects of winds, and the variation of electron temperature. Both studies appear to indicate that the original explanation is partially correct in that the rapid fall in T_e initiates a redistribution of ionization. However, to obtain as large an increase as that observed, it is necessary for the height of the layer peak to be raised by winds (or possibly electrodynamic drifts).

A second anomalous feature of the winter diurnal behavior is the predawn increase in density.[6] This feature seems far less pronounced in 1965 than in 1964, and is thought to disappear completely at sunspot maximum. Best evidence for it in these data is found in Figs. 8(k) and 8(l). An explanation offered for this phenomenon, in terms of downward diffusion of ionization from the protonosphere following conjugate sunset,[6] was discarded when it was recognized that during winter the region conjugate to Millstone remains sunlit throughout the night. (Direct evidence of this has been obtained from detection of photoelectrons arriving at Millstone Hill from the conjugate point during the winter night. This was accomplished by means of incoherent scatter observations of the plasma lines that the photoelectrons excite in the spectra of signals scattered by the F-region.[19])

For the latitude of Millstone, it is believed that the protonosphere can act as a source of ionization for the F-region throughout much of the night.[20] At equinox, the downward flux is thought to reach a peak of 10^{10} electrons/cm^2 about 1 hour after sunset, and thereafter decrease more or less monotonically. If the protonosphere is the source of the ionization seen in these nocturnal density increases, the reason for their occurrence in the early morning hours is not understood, but may be brought about by the more complicated temporal and spatial variation of the temperature of the field tube that must occur in winter.

During summer, the electron density at the layer peak usually reaches a maximum before noon, and a second much larger maximum at sunset. The transition from the characteristic winter to summer behavior occurs quite rapidly around equinox as may be seen by comparing Figs. 8(c) and 8(d). At Millstone, winter behavior is encountered from mid-October through March, and summer behavior from mid-April through September.

Reasons for the summer evening maximum have been discussed above. The depressed midday electron density in summer is thought to be caused by either or both the following effects: (1) a summer-to-winter change in the neutral composition of the atmosphere,[21-23] or (2) neutral winds which in the summer hemisphere blow away from the equator at noon and drive ionization down the field lines into regions of higher recombination rates.[15] Experimental evidence favoring

the first of these explanations has been obtained in the L-band incoherent scatter observations carried out at Millstone.[11,24] These appear to indicate that, relative to atomic oxygen (O^+), molecular ions (O_2^+ and NO^+) are present to greater altitudes in summer than in winter. Since the loss of ionization largely proceeds via the charge exchange reaction

$$O^+ + N_2 \rightarrow NO^+ + O$$

$$NO^+ + e \rightarrow N + O + h\nu \qquad (8)$$

this suggests that the abundance of the ionizable species (O) relative to molecular (O_2 and N_2) is lower in summer than in winter.

Duncan[25] recently reviewed all the explanations for the F-region seasonal anomally, and concluded that a variation in the neutral composition is the only one that will fit all the facts. He suggested that the change in composition is brought about by global transport of O from the summer to winter hemisphere. If this is the case, then it may be that effects (1) and (2) are related, and that a rapid changeover in the global wind pattern as the sun moves into the northern hemisphere causes the abrupt transition between the two types of behavior.

Changes in the relative abundance of O to N_2 in the F1-region could also be brought about by a change in the altitude (near 110 km) at which the atmosphere ceases to be mixed due to turbulence, and becomes one in which each species forms its own hydrostatic equilibrium distribution. Waldteufel[26] has found evidence for such changes from incoherent scatter studies of the ion-neutral collision frequency at 115 km. Continuation of these studies, together with more and better rocket measurements, are probably needed to resolve the relative importance of the various effects.

Support for the second explanation involving neutral winds has been provided by French incoherent scatter measurements of vertical drift velocity near the F-region peak.[27] However, although some seasonal variation of the wind velocity is found, it seems inadequate to account for the seasonal anomally.[28]

VI. ELECTRON AND ION TEMPERATURES

A. Mean Daytime and Nighttime T_e and T_i Profiles

In previous years, we attempted to present our temperature results in a manner analogous to the density results of Figs. 8(a-l), i.e., as isothermal contours drawn as functions of height and local time. This work has not been altogether very rewarding since, apart from somewhat complicated behavior in winter,[4,6] we tend to find that the temperatures remain fairly constant throughout the daytime and again during the nighttime. In addition, the transition between the two regimes is sufficiently rapid that it is doubtful whether it is properly explored in these measurements. This is especially true at dawn, where it has been necessary to carry out measurements restricted to a single altitude in order to obtain adequate time resolution.[8] Accordingly, in presenting the results for 1965, we have plotted only the average temperature profiles for the daytime (1000 to 1500 EST) and nighttime (2100 to 0300 EST). These are given in Figs. 11(a-k) and 12(a-k), respectively.

When drawing these curves, we have been guided by the height resolution of the measurements (indicated by the vertical bars) as well as the belief that electron, ion, and neutral temperatures are essentially the same below about 130 km (Refs. 11, 29, and 30). Therefore, both

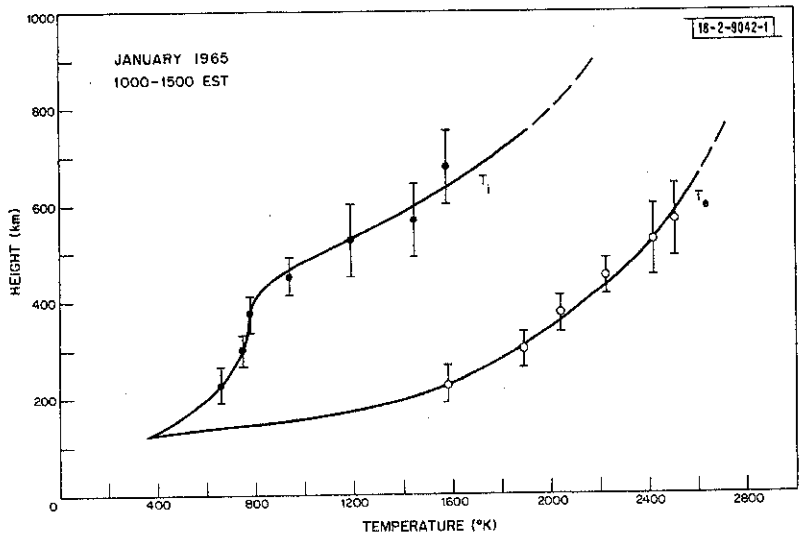

(a)

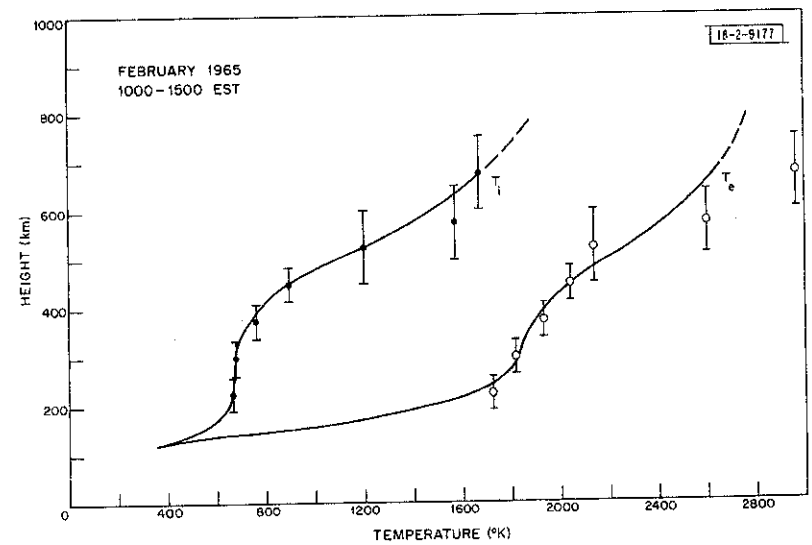

(b)

Fig. 11(a-k). Mean daytime electron- and ion-temperature profiles. These plots obtained by averaging all measurements between 1000 and 1500 EST. Bars denote height of exploring pulse. From July onwards, ion temperature between 300 and 500 km has been underestimated (see Sec. IV-D).

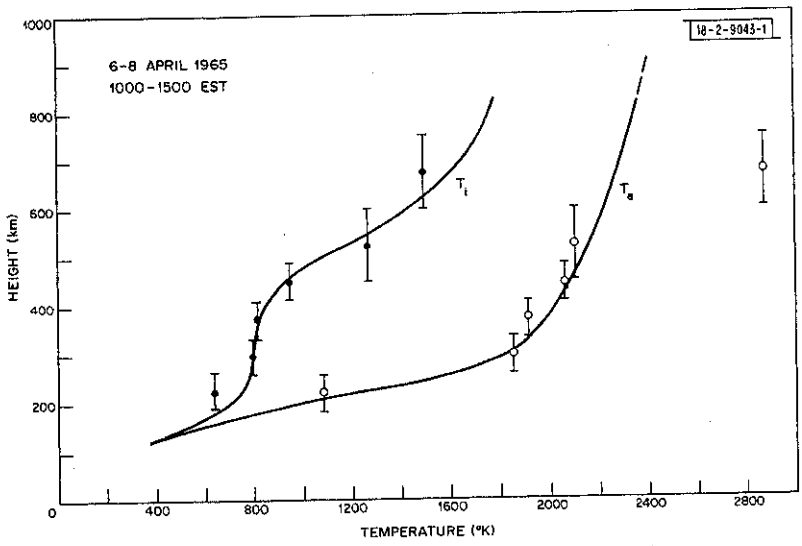

(c)

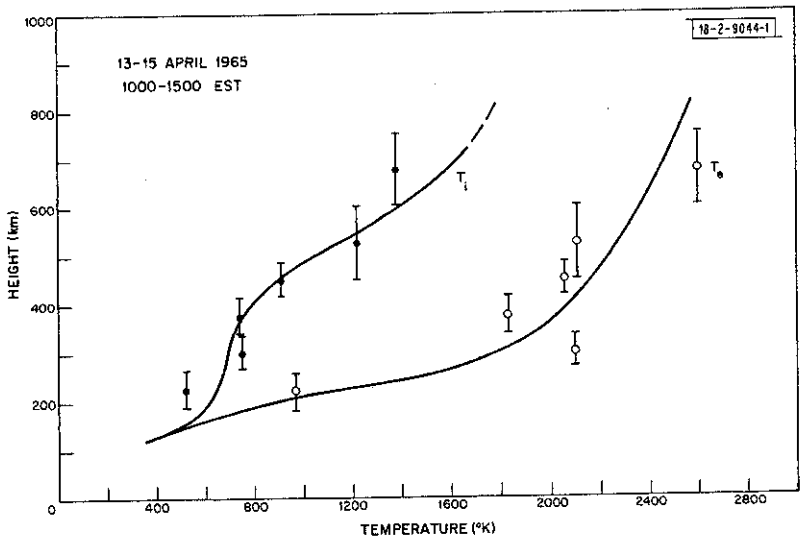

(d)

Fig. 11(a-k). Continued.

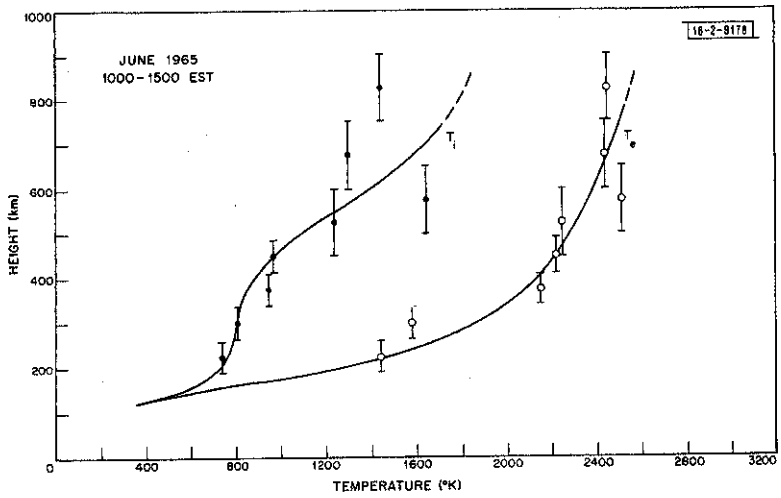

(e)

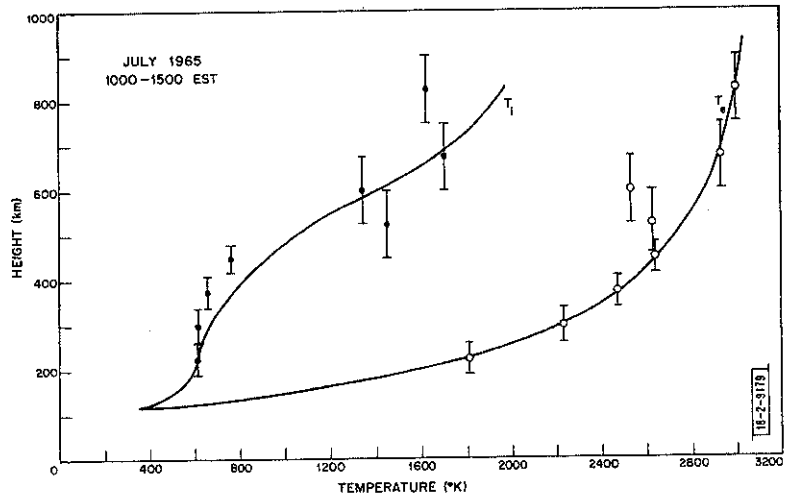

(f)

Fig. 11(a-k). Continued.

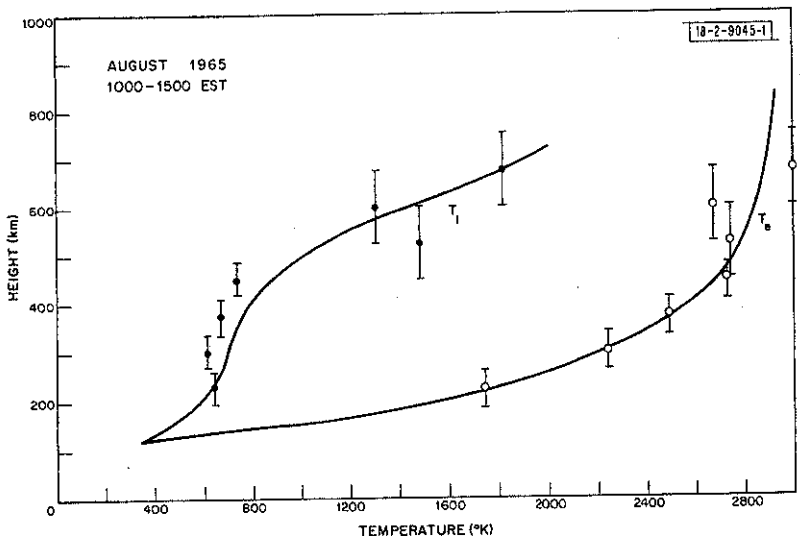

(g)

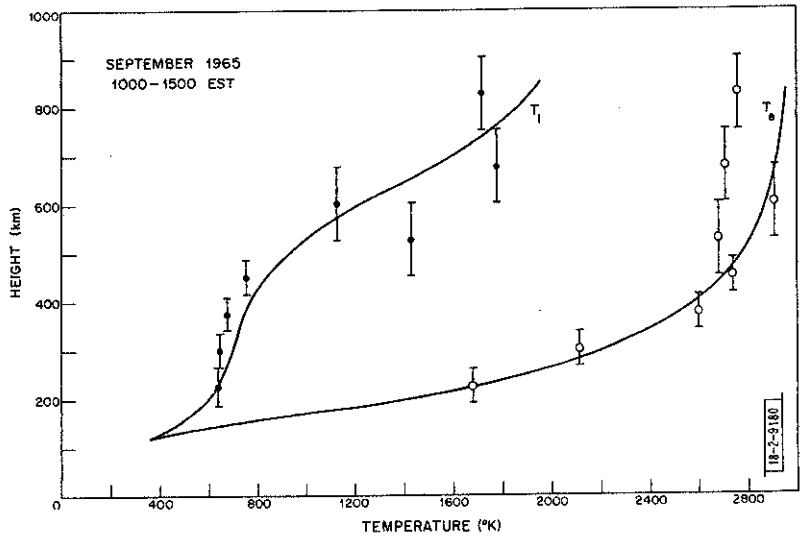

(h)

Fig. 11(a-k). Continued.

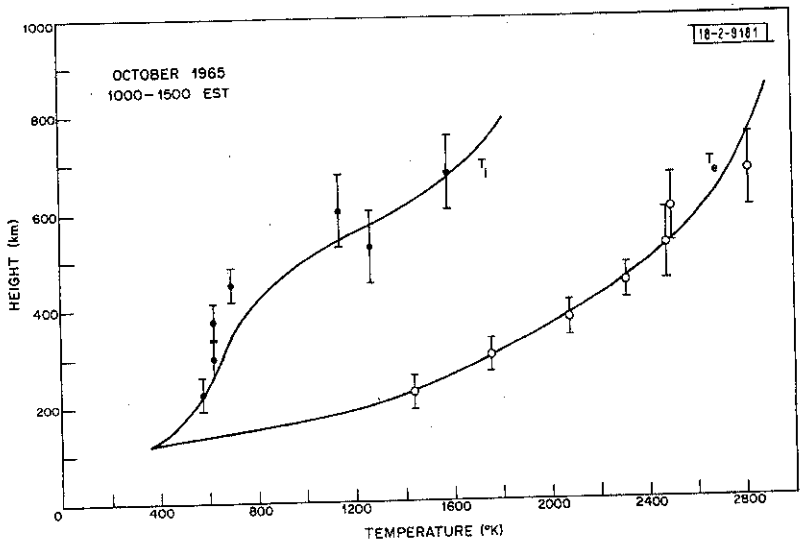

(i)

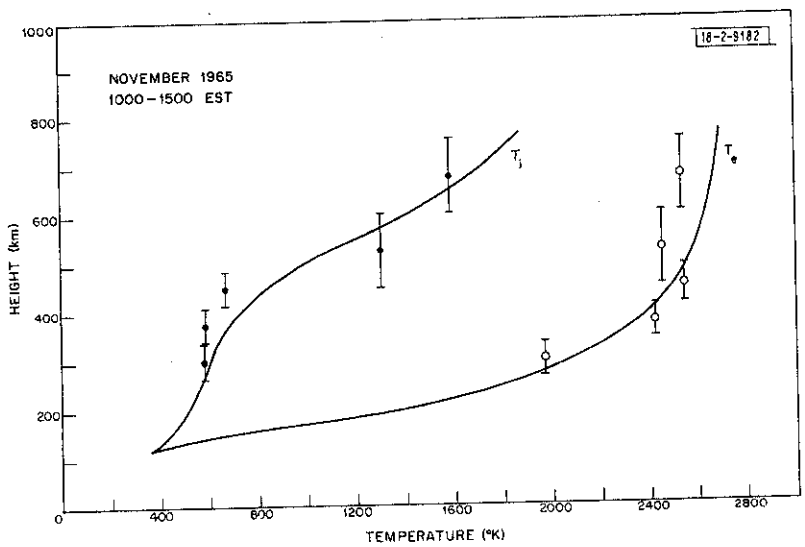

(j)

Fig. 11(a-k). Continued.

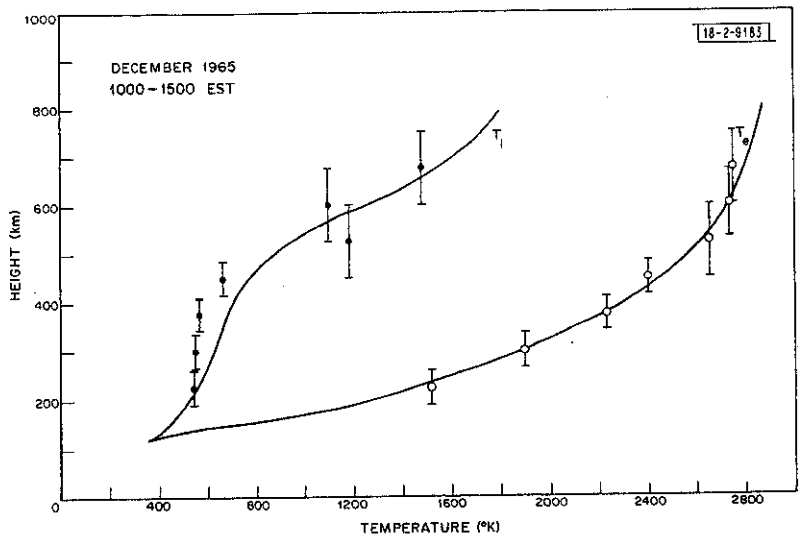

(k)

Fig. 11(a-k). Continued.

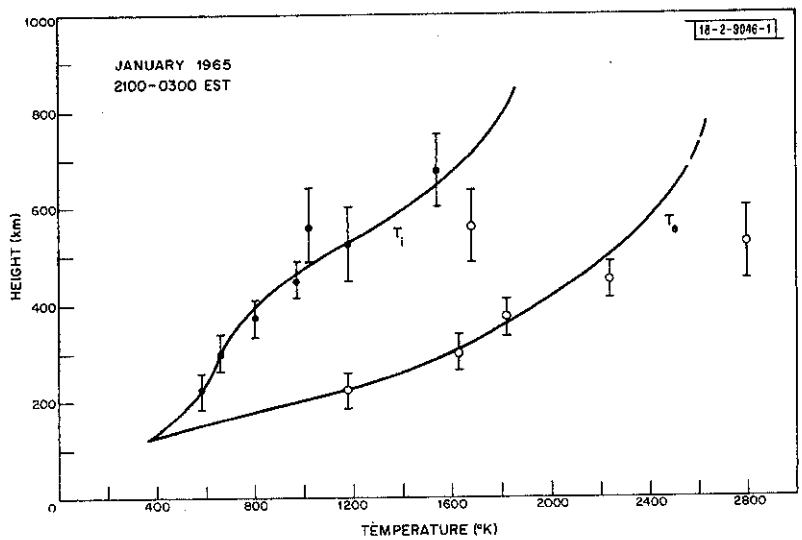

(a)

Fig. 12(a-k). Mean nighttime electron- and ion-temperature profiles. These plots obtained by averaging all measurements between 2100 and 0300 EST. Bars denote height of exploring pulse.

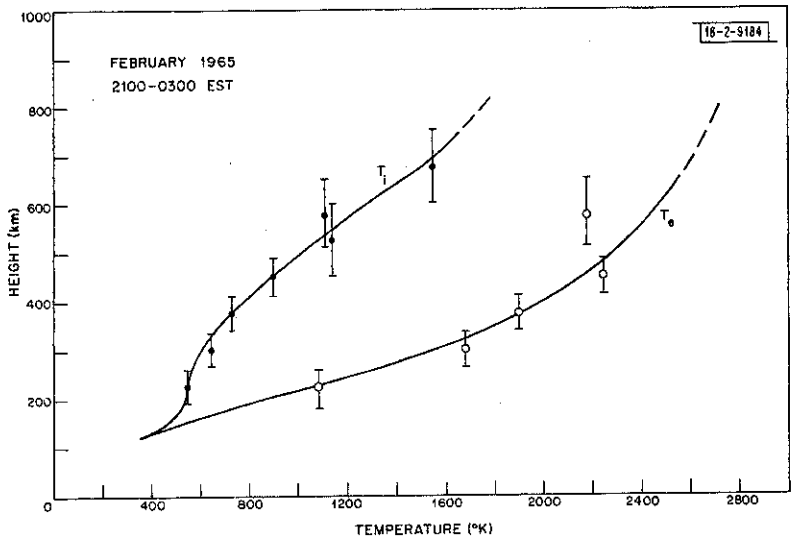

(b)

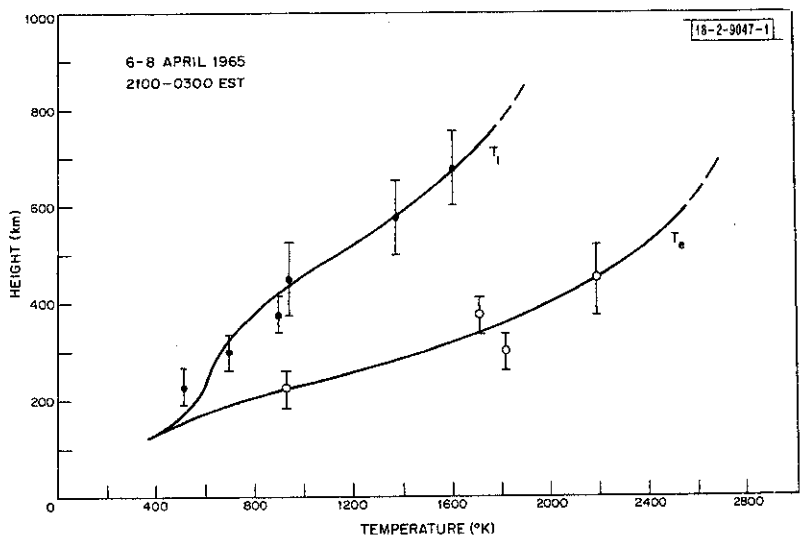

(c)

Fig. 12(a-k). Continued.

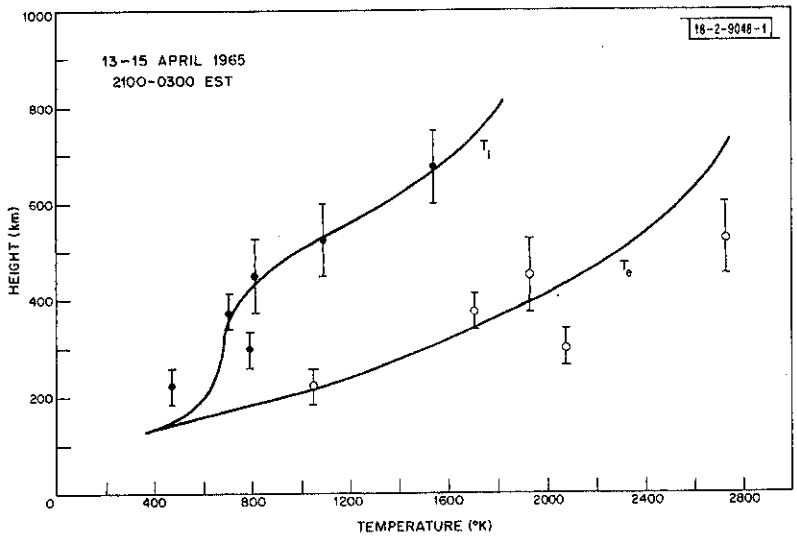

(d)

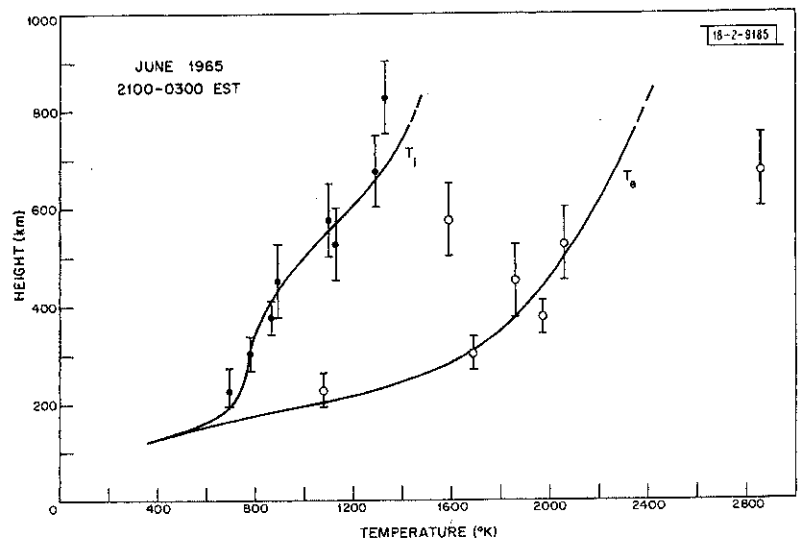

(e)

Fig. 12(a-k). Continued.

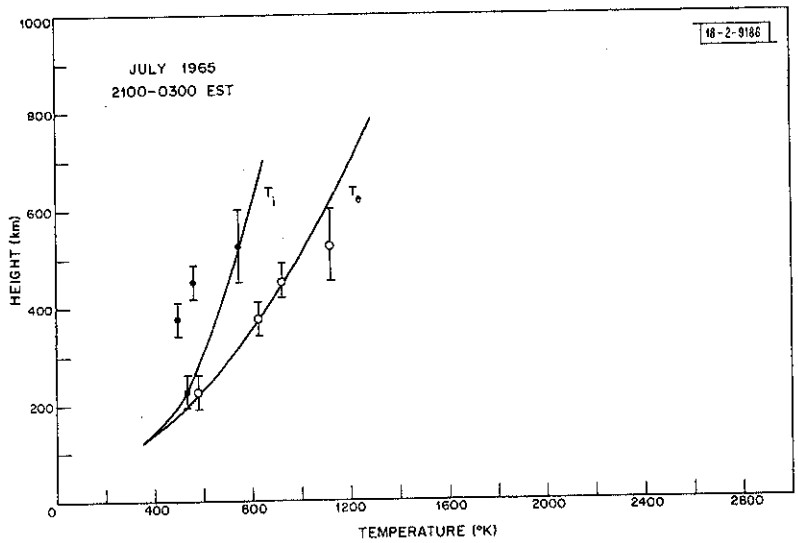

(f)

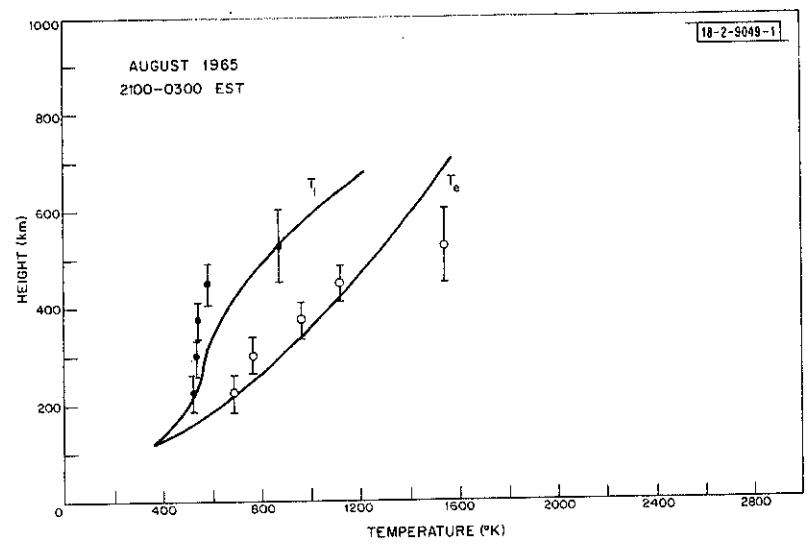

(g)

Fig. 12(a-k). Continued.

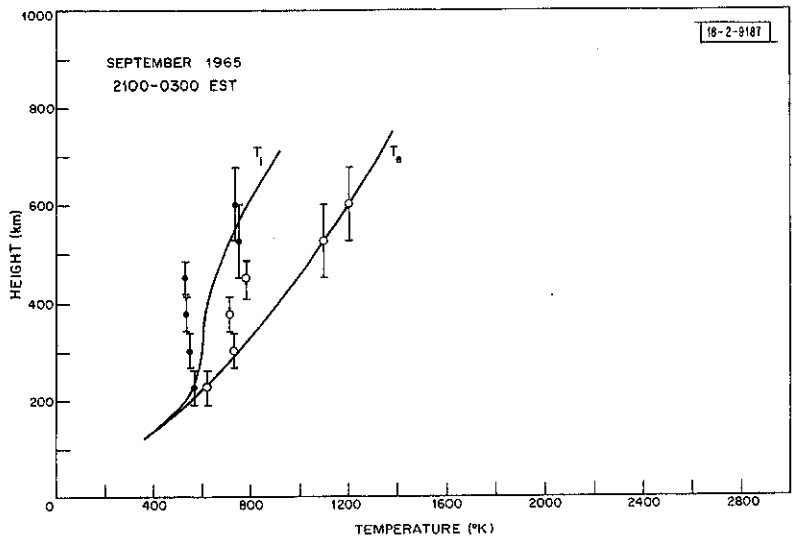

(h)

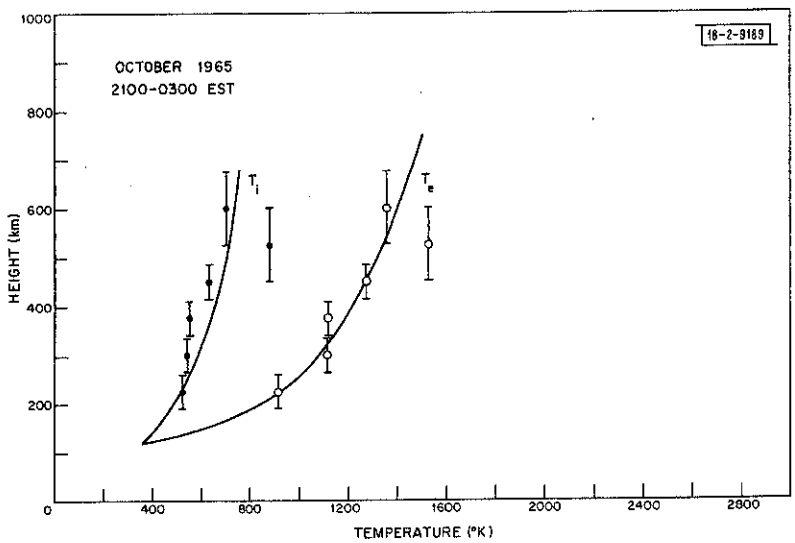

(i)

Fig. 12(a-k). Continued.

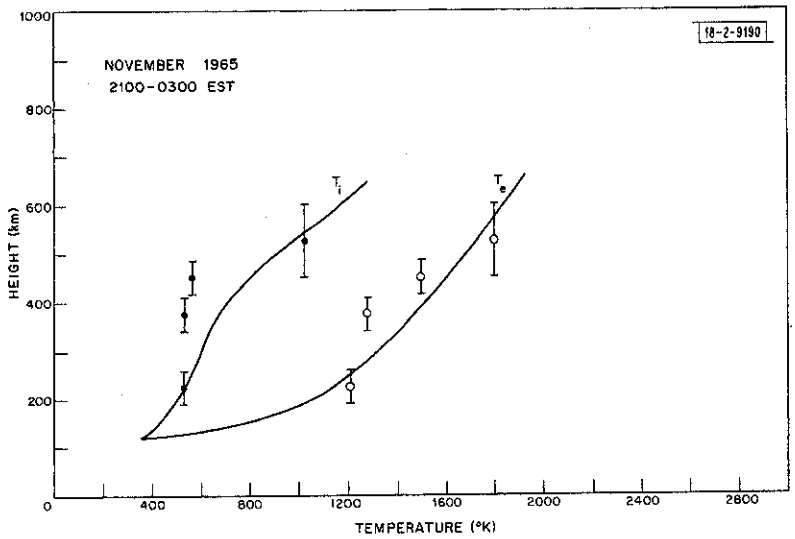

(j)

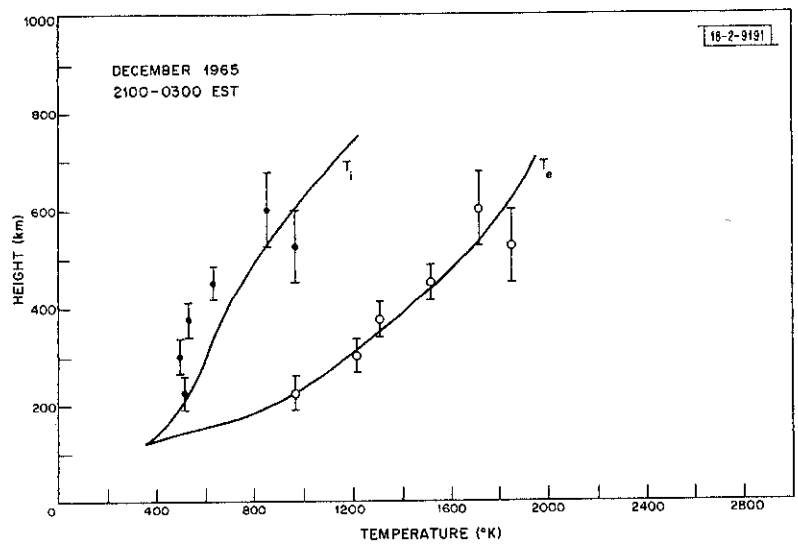

(k)

Fig. 12(a-k). Continued.

T_e and T_i have been extrapolated downward to the value of 355°K employed as the temperature at 120 km in the CIRA 1965 model atmospheres.

For the daytime results obtained after June [Figs. 11(f-k)], the curve for T_i has been drawn through the point at 225 km, and then taken higher than the plotted values to compensate for the underestimate in T_i (Sec. IV-D). However, it seems doubtful that this portion of the curve is very accurate as the exospheric temperature during these months is thought to have been of the order of 800°K or higher.[11] As noted earlier, the electron temperature should be substantially independent of the error in T_i.

B. Discussion

The temperature behavior observed at Millstone has been discussed previously.[4] Some of the photoelectrons created in the process of ion production in the atmosphere have sufficient energy to escape the local ionosphere completely. Thus, during the daytime, an upward flux of photoelectrons is established that traverses the protonosphere to the conjugate ionosphere. This escaping photoelectron flux deposits some of its energy in the protonosphere via Coulomb encounters with the ambient electrons. The balance of the energy is presumed to be given directly to the conjugate ionosphere. In order to account for the large daytime temperature gradients seen in the electron temperature, we earlier postulated that this effect gave rise to a heat flux conducted into the ionosphere on the order of 5×10^9 eV/cm^2/sec (Refs. 7 and 31), and assumed that the escaping energy flux was even larger. Recent theoretical estimates of the magnitude of the escape flux have given general support to this conclusion.[32-35]

A number of studies of the F-region thermal behavior have been carried out in which a direct comparison has been made with the Millstone measurements.[35-37] In the most recent of these,[35,37] the effects of photoelectron escape and fine-structure cooling of oxygen were both included. Despite the enormous sophistication of these models, differences remain between the theory and the measurements. However, these may simply result from uncertainties in the photoionization cross sections, collision cross sections, and other parameters that were employed in the calculations.[35] For example, it was found that the results of the two studies differ more widely between themselves than with the measurements.[35]

One phenomenon that has recently come to light and is not adequately included in any of the existing models is the importance of elastic encounters between photoelectrons and neutral particles. These encounters serve to limit the escape flux, as pointed out by Nisbet.[34] In addition, they cause a portion of the flux of photoelectrons arriving from the conjugate hemisphere to be backscattered[19,38-40] so that not all the arriving photoelectrons will deposit their energy in the local ionosphere. The albedo of the atmosphere is possibly as high as 0.5 (Ref. 41) causing many of the photoelectrons to make several traversals of the protonosphere before losing all their energy or penetrating into the F-region at one end. This must cause a larger fraction of the energy of the escaping photoelectrons to appear in the form of heat conducted along the field line,[38] and suggests that the escape flux can be determined from the temperature gradient observed at high altitudes more accurately than was previously thought.

The photoelectron escape flux is believed to be responsible for the high temperatures observed at Millstone during the winter nights[4,6,7] because at this time the region conjugate to Millstone is still sunlit and supplies heat to the protonosphere.[8] It is not certain how much heat is deposited directly in the local ionosphere by arriving photoelectrons, but heat conducted from the protonosphere is on the order of half the daytime value.[7] Observations of the plasma lines

in the spectrum of the Thomson scatter signals from the F-region during the winter nights show conclusively that photoelectrons do reach Millstone in significant numbers.[19] However, plasma lines are observed only above $h_{max}F2$, indicating that whatever energy the photoelectrons deposit is introduced at rather high altitudes.

During the summer nights, a small temperature difference appears to persist between electrons and ions and this is thought to be maintained by the cooling of the protonosphere.[20,42] As pointed out by Geisler and Bowhill,[42] the protonosphere is heated during the daytime to a temperature above that of the F-region, and at nighttime continues to warm the F-region as it cools. Since the heat conductivity varies with electron temperature as $T_e^{5/2}$, the lowering of the F-region temperature "chokes off" the heat loss, permitting the protonosphere to continue to warm the F-region for many hours after sunset. Additional heat is brought into the F-region via transport of electrons (convection) to lower altitudes[20] under the influence of the reduced hydrostatic pressure below. For the latitude of Millstone, this process is thought to be less effective than thermal conduction, but quite important nevertheless.[20]

VII. MAGNETIC DISTURBANCE EFFECTS

A. August and September

The average magnetic K_p figures given in Table III are for the entire period of observation. In August and September, the first 24-hours' observations were relatively quiet periods and were followed by disturbed periods. These months therefore afford the opportunity for making a direct comparison of consecutive quiet and disturbed periods. In order to do this, we have recomputed the daytime and nighttime temperature averages for these months, separating the quiet and disturbed days. The results are presented in Figs. 13(a-b) and 14(a-b) for the two months.

The August storm appears to have been one of the principal storms of 1965 (Ref. 43), with a sudden commencement (SC) at 0840 EST on 18 August and lasting for the following 5 days. Despite this, comparison of Fig. 13(a) shows little difference between the daytime temperatures observed on 17 and 18 August. The slightly lower electron temperature observed on the storm day [Fig. 13(a)] may have been caused by the slightly higher electron densities encountered on that day [Fig. 6(h)]. It would seem that the observations conducted on 18 August followed too soon after the sudden commencement for significant heating of the atmosphere to have taken place.[44] The behavior averaged over the periods 2100 to 0300 EST for the nights of 17-18 and 18-19 August is compared in Fig. 13(b). There appears to be a distinct increase in the ion temperature but no dramatic increase in electron temperature as encountered at nighttime in September 1964 (Ref. 10).

The September storm began at 0954 EST on 15 September and lasted about 4 days.[43] Here again, the time interval between the commencement of the storm and the daytime observations seems to have been too short for significant changes to have been produced in the temperature distribution, although the ion temperature does appear to be higher on the disturbed day [Fig. 14(a)]. A comparison of the nighttime behavior for quiet and disturbed periods [Fig. 14(b)] also shows little difference.

B. June

As already noted, the observations made in June were the most disturbed for the entire year. A sudden commencement occurred at ~0600 EST on 15 June, but the magnetic indices A_p and K_p

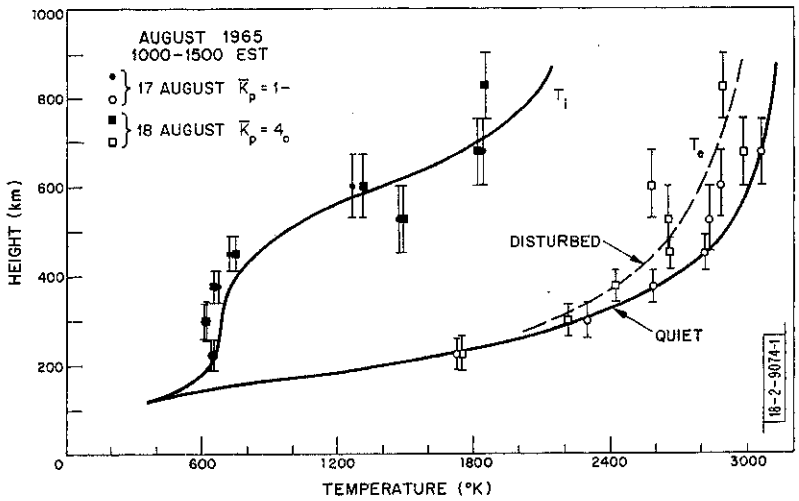

(a) Daytime.

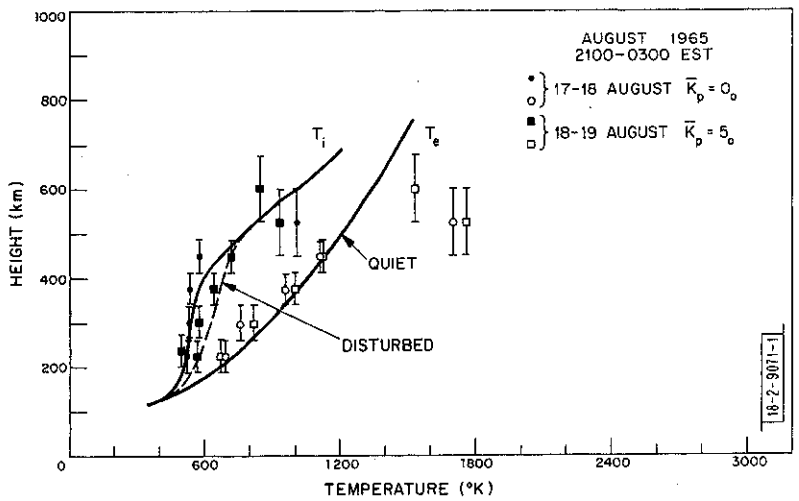

(b) Nighttime.

Fig. 13(a-b). Comparison of mean temperature profiles for quiet and disturbed periods in August. $\bar{K}_p$ is mean value of K_p index over these time intervals.

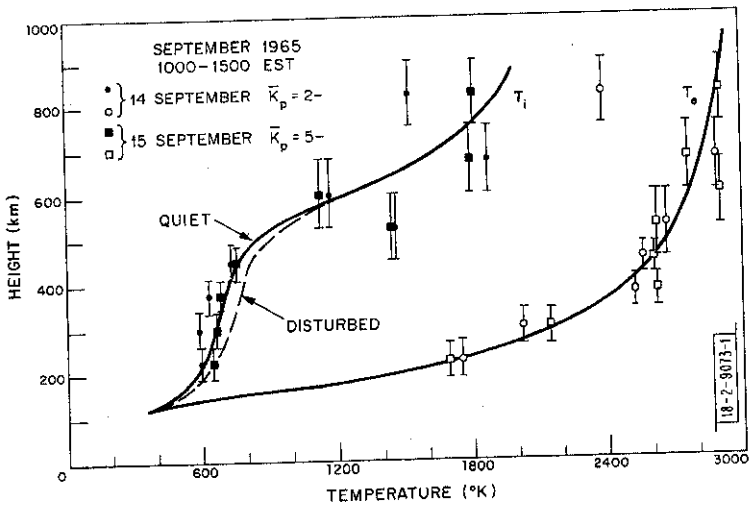

(a) Daytime.

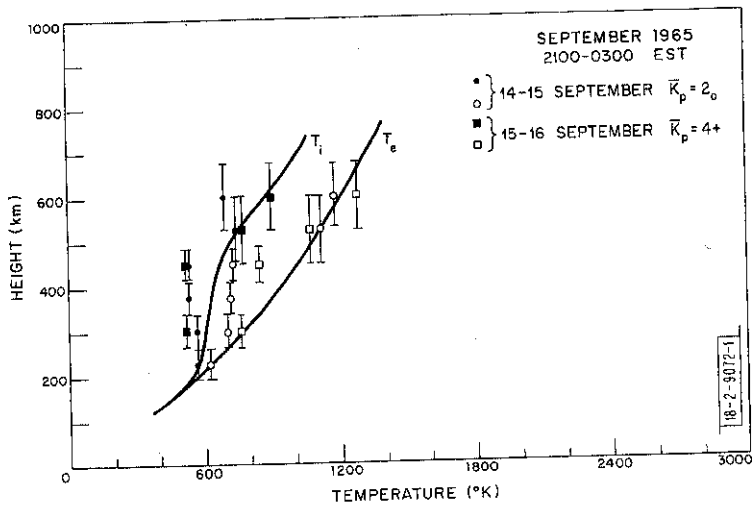

(b) Nighttime.

Fig. 14(a-b). Comparison of mean temperature profiles for quiet and disturbed periods in September. $\bar{K}_p$ is mean value of K_p index over these time intervals.

reached their highest values on 16 June. The electron density observed on the 16th was considerably depressed compared with that on the 15th [Figs. 6(f) and 8(f)] except for the period around sunset. At nighttime, the electron density fell to anomalously low values for the time of year, suggesting that the trough of low ionization observed by the satellite Alouette[45] had moved over Millstone. Figures 15(a-b) compare the average daytime and nighttime temperatures for June and July. Here, the storm effects are clearly evident. During the daytime, the ion temperature had been increased and the electron temperature reduced. At nighttime, T_e and T_i were both increased. [The June values of T_i are not plotted in Fig. 15(b) because they fall on the July T_e curve.]

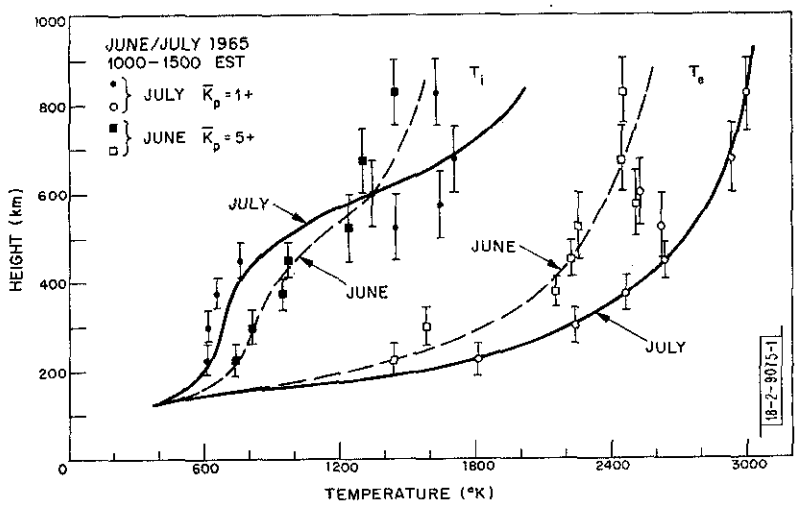

(a) Daytime.

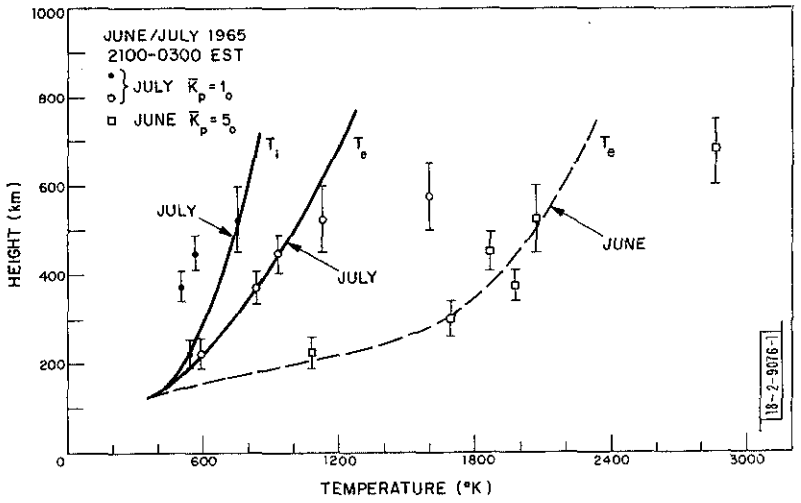

(b) Nighttime.

Fig. 15(a-b). Comparison of mean temperature profiles for June (disturbed days) and July (quiet days). $\bar{K}_p$ is mean value of K_p index over these time intervals.

C. Discussion

In agreement with conclusions reached earlier,[10] it appears that the principal daytime effect of disturbed conditions is to raise the exospheric neutral temperature, and consequently the ion temperature, at altitudes where the ion and neutral temperatures are substantially the same (i.e., below about 400 km). This seems very clear from Fig. 15(a). Above ~600 km, this difference seems to disappear since at this altitude the electron temperature begins to govern the ion temperature.

A reduction in the daytime electron temperature was not observed in September 1964, but did occur in June 1965. Owing to the expansion of the neutral atmosphere, the F-layer appears to have been formed higher in June than in July [compare Figs. 8(f) and (g) or 9(d) and (e)]. As a result, the electron density N is actually higher at altitudes in the range 300 to 500 km in June than in July. This would lead to increased local cooling of the electrons by the ions, which proceeds at a rate proportional to $N^2(T_e - T_i)/T_e^{3/2}$, and may account for the decrease in electron temperature.

The very large evening maximum observed on 15 and 16 June must be attributed to the fact that at sunset on both days the layer height was very large, either as a result of increased neutral wind velocity or, as seems more likely, the action of an east-west electric field.

The very low peak electron density observed on 16 June prior to sunset supports the view proposed by Duncan,[25] Norton,[46] and others that at midlatitudes the storm time behavior resembles the winter-to-summer transition because abnormally low F-region electron densities are then often encountered. These authors attribute the storm behavior to the same basic cause as the seasonal anomally, namely, a decrease in the ratio of O to N_2 (and O_2) at F-region heights.

The June 1965 nighttime behavior closely resembles that observed in September 1964 in that very high electron temperatures were encountered. On the other hand, this was not observed in August [Fig. 13(b)] although the average K_p value was 5_o in both cases. We speculate that in June the ionization trough,[45] which appears to mark the boundary between the regular midlatitude ionosphere and the irregular polar region, moved southward over Millstone. Norton and Marovich[47] have observed that the trough appears to be associated with the midlatitude red arc, and that high plasma temperatures exist inside the trough. If this is the case, the difference between the August and June nights could be explained by different locations of the trough with respect to Millstone.

VIII. SUMMARY AND CONCLUSIONS

The Millstone Hill UHF Thomson scatter radar system was operated routinely throughout 1965 to obtain F-region electron densities and electron and ion temperatures. Measurements were usually made for 48-hour periods on the Geophysical World Days near the middle of each month. Magnetic storm sudden commencements occurred during two of the observing periods (August and September) and immediately prior to the observations in June. However, storm-type behavior is clearly evident only in the case of the June measurements. During the remaining months, the magnetic activity was low and the results differ little from those observed the previous year (sunspot minimum).

Millstone is a midlatitude station that exhibits a characteristic winter and summer electron density behavior, with a rapid transition between the two near equinox. This seasonal variation of electron density is not accompanied by marked variations in either the electron or the ion

temperature. The depressed electron density encountered in summer is thought to result from a change in the neutral composition of the atmosphere, although confirmation of this from rocket results is still lacking. The storm behavior observed in June is thought to represent the same type of composition change, but in extreme form. Global transport of atomic oxygen and changes of the turbopause altitude have both been advanced as mechanisms which produce this composition change.

In contrast to the uncertainties that still exist concerning the mechanisms governing the behavior of the electron density, the thermal structure of the F-region seems reasonably well understood. Although a perfect match between theory and measurement has not yet been demonstrated, we feel that uncertainty concerning the absolute magnitude of various parameters employed in the theory is the chief source of remaining error.

The measurements at Millstone are capable of a number of improvements including (a) extensions both to higher and lower altitudes, (b) improvements in accuracy – especially in determining the ion temperature, and (c) increased time and height resolution. Most of these requirements were met recently by the construction of a new spectrum analyzer, and by modifications to permit observations (at low altitudes) using short-pulse autocorrelation methods of spectrum measurements.

ACKNOWLEDGMENTS

The invaluable assistance of W. A. Reid, J. H. McNally, J. Morin, and others at the Millstone Hill Radar Observatory in maintaining, modifying, and operating the radar equipment for these measurements is gratefully acknowledged. R. Julian and J. Moriello contributed extensively to the data reduction by writing the computer program employed to analyze the measured signal spectra. J. K. Upham carried out the computer processing of these data, while the data reduction requiring hand analysis was chiefly performed by Misses D. Tourigny, F. Angier, and L. Zak. The constant support of P. B. Sebring is also gratefully acknowledged.

REFERENCES

1. J.V. Evans, "Ionospheric Backscatter Observations at Millstone Hill," Technical Report 374, Lincoln Laboratory, M.I.T. (22 January 1965), DDC AD-616607.
2. _____, "Millstone Hill Thomson Scatter Results for 1964," Technical Report 430, Lincoln Laboratory, M.I.T. (15 November 1967), DDC AD-668436.
3. _____, Planet. Space Sci. 13, 1031 (1965), DDC AD-616607.
4. _____, Planet. Space Sci. 15, 1387 (1967).
5. _____, J. Geophys. Res. 70, 1175 (1965), DDC AD-614310.
6. _____, J. Geophys. Res. 70, 4331 (1965), DDC AD-623606.
7. _____, Planet. Space Sci. 15, 1557 (1967).
8. _____, J. Geophys. Res. 73, 3489 (1968), DDC AD-673605.
9. _____, J. Geophys. Res. 70, 131 (1965), DDC AD-613886.
10. _____, J. Geophys. Res. 70, 2726 (1965), DDC AD-621233.
11. _____ and L.P. Cox, J. Geophys. Res. 75, 159 (1970), DDC AD-703492.
12. G.R. Thomas and F.H. Venables, J. Atmos. Terrest. Phys. 29, 621 (1967).
13. A.L. Schmeltekopf, F.C. Fehsenfeld, G.I. Gilman and E.E. Ferguson, Planet. Space Sci. 15, 401 (1967).
14. G.R. Thomas, J. Atmos. Terrest. Phys. 30, 1429 (1968).
15. H. Kohl and J.W. King, J. Atmos. Terrest. Phys. 29, 1045 (1967).
16. H. Kohl, J.W. King and D. Eccles, J. Atmos. Terrest. Phys. 30, 1733 (1968).
17. D.F. Strobel, "On the Ionospheric F2-Layer and Its Maintenance at Night by Thermospheric Winds," PhD. Thesis, Department of Applied Physics, Harvard University (1968).
18. D.L. Sterling, W.B. Hanson, R.J. Moffett and R.G. Baxter, Radio Sci. 4, 1005 (1969).
19. J.V. Evans and I.J. Gastman, J. Geophys. Res. 75, 807 (1970).
20. A.F. Nagy, P. Bauer and E.G. Fontheim, J. Geophys. Res. 73, 6259 (1968).
21. M. Rishbeth and C.S.G.K. Setty, J. Atmos. Terrest. Phys. 20, 263 (1961).
22. J.W. Wright, J. Geophys. Res. 68, 4379 (1963).
23. W. Becker, Electron Density Profiles in the Ionosphere and Exosphere, J. Frihagen, ed. (North-Holland Publishing Co., Amsterdam, 1966), p. 218.
24. J.V. Evans, J. Geophys. Res. 72, 3343 (1967), DDC AD-658912.
25. R.A. Duncan, J. Atmos. Terrest. Phys. 31, 59 (1969).
26. P. Waldteufel, personal communication (1969).
27. G. Vasseur, J. Atmos. Terrest. Phys. 31, 397 (1969).
28. _____, J. Atmos. Terrest. Phys. (in press, 1970).
29. H. Carru, M. Petit and P. Waldteufel, J. Atmos. Terrest. Phys. 29, 351 (1967).
30. R.H. Wand and F.W. Perkins, J. Geophys. Res. 73, 6370 (1968).
31. J.V. Evans and G.P. Mantas, J. Atmos. Terrest. Phys. 30, 563 (1968).
32. E.G. Fontheim, A.E. Beutler and A.F. Nagy, Ann. Geophys. 24, 489 (1968).
33. M.L. Duboin, G. Lejeune, M. Petit and G. Weill, J. Atmos. Terrest. Phys. 30, 299 (1968).
34. J.S. Nisbet, J. Atmos. Terrest. Phys. 30, 1257 (1968).
35. A.F. Nagy, E.G. Fontheim, R.S. Stolarski and A.E. Beutler, J. Geophys. Res. 74, 4667 (1969).
36. A. Dalgarno, M.B. McElroy and J.C.G. Walker, Planet. Space Sci. 15, 331 (1967).
37. A. Dalgarno, M.B. McElroy, M.H. Rees and J.C.G. Walker, Planet. Space Sci. 16, 1371 (1968).
38. P.M. Banks and A.F. Nagy, J. Geophys. Res. 75, 1902 (1970).

39. R.J. Cicerone and S.A. Bowhill, Radio Sci. 5, 49 (1970).
40. B.C. Narasinga Rao and E.J.R. Maier, J. Geophys. Res. (in press, 1970).
41. R.J. Cicerone, private communication (1969).
42. J.E. Geisler and S.A. Bowhill, J. Atmos. Terrest. Phys. 27, 119 (1965).
43. J.V. Lincoln, J. Geophys. Res. 71, 975 (1966).
44. L.G. Jacchia, Space Res. VIII, 800 (1968).
45. D.B. Muldrew, J. Geophys. Res. 70, 2635 (1965).
46. R.B. Norton, Proc. IEEE 57, 1147 (1969).
47. R.B. Norton and E. Marovich, Proc. IEEE 57, 1158 (1969).

DOCUMENT CONTROL DATA – R&D

(Security classification of title, body of abstract and indexing annotation must be entered when the overall report is classified)

1. ORIGINATING ACTIVITY *(Corporate author)* Lincoln Laboratory, M.I.T.	2a. REPORT SECURITY CLASSIFICATION Unclassified 2b. GROUP None

3. REPORT TITLE

Millstone Hill Thomson Scatter Results for 1965

4. DESCRIPTIVE NOTES *(Type of report and inclusive dates)*

Technical Report

5. AUTHOR(S) *(Last name, first name, initial)*

Evans, John V.

6. REPORT DATE	7a. TOTAL NO. OF PAGES	7b. NO. OF REFS
8 December 1969	56	47

8a. CONTRACT OR GRANT NO. AF 19(628)-5167 b. PROJECT NO. 649L c. d.	9a. ORIGINATOR'S REPORT NUMBER(S) Technical Report 474 9b. OTHER REPORT NO(S) *(Any other numbers that may be assigned this report)* ESD-TR-69-387

10. AVAILABILITY/LIMITATION NOTICES

This document has been approved for public release and sale; its distribution is unlimited.

11. SUPPLEMENTARY NOTES	12. SPONSORING MILITARY ACTIVITY
None	Air Force Systems Command, USAF

13. ABSTRACT

This report presents F-region electron densities, and electron and ion temperatures observed during the year 1965 at the Millstone Hill Radar Observatory (42.6°N, 71.5°W) by the UHF Thomson (incoherent) scatter radar. The measurements were made over 48-hour periods that were usually scheduled to include the International Geophysical World days near the center of each month. Geomagnetic storm sudden commencements occurred during two of the observing periods, but do not appear to have given rise to marked variation of the densities or temperatures. On the other hand, measurements made during the progress of a major storm (15-19 June 1965) exhibit large changes compared with the behavior observed in the following month. The remaining months were magnetically quiet, and the density and temperature behavior were similar to those observed in 1964. Millstone is a midlatitude station exhibiting a characteristic "winter" and "summer" daytime density variation. The transition between these two types occurs rapidly around equinox, without any corresponding seasonal change in the F-region thermal structure. Current ideas concerning the mechanisms responsible for this and other features of diurnal and seasonal variations are discussed.

14. KEY WORDS

Millstone radar
F-region
diurnal variations
electron density
ionospheric scatter
seasonal variations
temperature effects
spectrum analyzers